Article

Cell Metabolism

Glutamine Links Obesity to Inflammation in Human White Adipose Tissue

Graphical Abstract

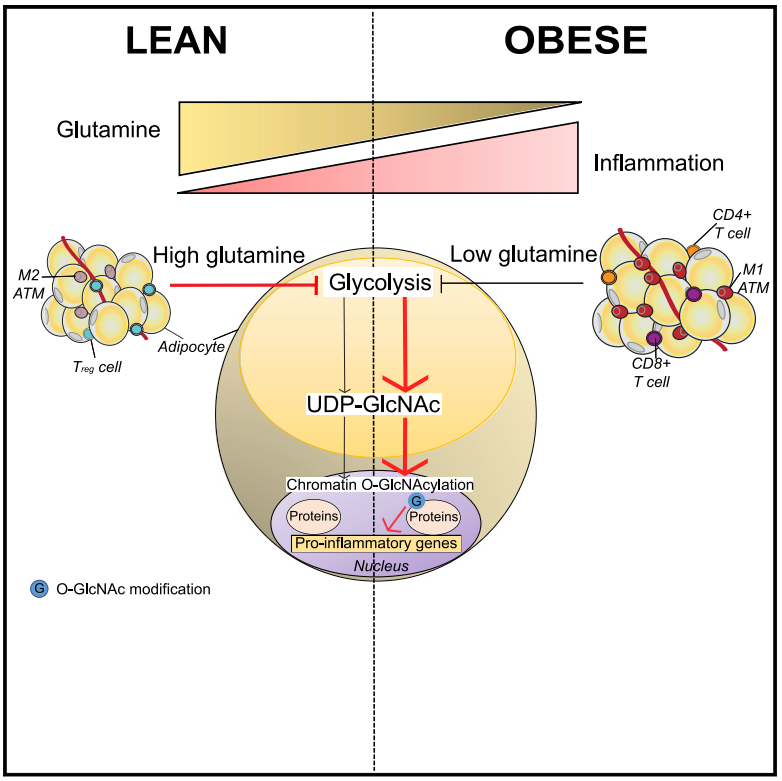

Highlights

- Human adipose glutamine levels correlate inversely with fat mass and inflammation
- Glutamine administration to mice attenuates adipose tissue inflammation
- High glutamine reduces glycolysis and inflammation in human fat cells *in vitro*
- Nuclear O-GlcNAcylation links glutamine to inflammation in adipose tissue

Authors

Paul Petrus, Simon Lecoutre, Lucile Dollet, ..., Myriam Aouadi, Anna Krook, Mikael Rydén

Correspondence

mikael.ryden@ki.se

In Brief

Obesity is linked to white adipose tissue inflammation, but the causal factors remain unclear. Based on data obtained from clinical cohorts, mouse models, and cell cultures, Petrus et al. show that a reduction of adipose tissue glutamine levels in obesity leads to increased nuclear O-GlcNAcylation in adipocytes, which induces transcriptional activity of pro-inflammatory pathways.

Petrus et al., 2020, Cell Metabolism *31*, 375–390
February 4, 2020
https://doi.org/10.1016/j.cmet.2019.11.019

CellPress

Cell Metabolism
Article

Glutamine Links Obesity to Inflammation in Human White Adipose Tissue

Paul Petrus,[1,12] Simon Lecoutre,[1,12] Lucile Dollet,[2] Clotilde Wiel,[3] André Sulen,[4] Hui Gao,[1] Beatriz Tavira,[1] Jurga Laurencikiene,[1] Olav Rooyackers,[5] Antonio Checa,[6] Iyadh Douagi,[1] Craig E. Wheelock,[6] Peter Arner,[1] Mark McCarthy,[7,8,9,11] Martin O. Bergo,[3] Laurienne Edgar,[10] Robin P. Choudhury,[10] Myriam Aouadi,[4] Anna Krook,[2] and Mikael Rydén[1,13,*]

[1]Department of Medicine (H7), Karolinska Institutet, Stockholm 141 86, Sweden
[2]Department of Physiology and Pharmacology, Integrative Physiology, Karolinska Institutet, Stockholm, Sweden
[3]Department of Biosciences and Nutrition (BioNut), H2, Karolinska Institutet, Stockholm 141 86, Sweden
[4]Integrated Cardio Metabolic Centre, Department of Medicine, Karolinska Institutet, Huddinge, Sweden
[5]Perioperative Medicine and Intensive Care, B31, Karolinska University Hospital, Huddinge, 141 86 Stockholm, Sweden
[6]Department of Medical Biochemistry and Biophysics, Karolinska Institutet, 171 77 Stockholm, Sweden
[7]Oxford Centre for Diabetes, Endocrinology and Metabolism, University of Oxford, Churchill Hospital, Old Road, Headington, Oxford OX3 7LJ, UK
[8]Wellcome Centre for Human Genetics, University of Oxford, Roosevelt Drive, Oxford OX3 7BN, UK
[9]Oxford NIHR Biomedical Research Centre, Oxford University Hospitals NHS Foundation Trust, John Radcliffe Hospital, Oxford OX3 9DU, UK
[10]Division of Cardiovascular Medicine, Radcliffe Department of Medicine, University of Oxford, Oxford, UK
[11]Present address: Genentech, 340 Point San Bruno Boulevard, South San Francisco, CA 94080, USA
[12]These authors contributed equally
[13]Lead Contact
*Correspondence: mikael.ryden@ki.se
https://doi.org/10.1016/j.cmet.2019.11.019

SUMMARY

While obesity and associated metabolic complications are linked to inflammation of white adipose tissue (WAT), the causal factors remain unclear. We hypothesized that the local metabolic environment could be an important determinant. To this end, we compared metabolites released from WAT of 81 obese and non-obese women. This identified glutamine to be downregulated in obesity and inversely associated with a pernicious WAT phenotype. Glutamine administration *in vitro* and *in vivo* attenuated both pro-inflammatory gene and protein levels in adipocytes and WAT and macrophage infiltration in WAT. Metabolomic and bioenergetic analyses in human adipocytes suggested that glutamine attenuated glycolysis and reduced uridine diphosphate N-acetylglucosamine (UDP-GlcNAc) levels. UDP-GlcNAc is the substrate for the post-translational modification O-linked β-N-acetylglucosamine (O-GlcNAc) mediated by the enzyme O-GlcNAc transferase. Functional studies in human adipocytes established a mechanistic link between reduced glutamine, O-GlcNAcylation of nuclear proteins, and a pro-inflammatory transcriptional response. Altogether, glutamine metabolism is linked to WAT inflammation in obesity.

INTRODUCTION

Our current lifestyle facilitates caloric oversupply (Hill et al., 2003), where energy is stored as triglycerides in white adipose tissue (WAT). Excess WAT mass leads to increased fat cell size (hypertrophy) and a chronic low-grade inflammation (Crewe et al., 2017; Hotamisligil, 2006; Rosen and Spiegelman, 2014). These changes are closely linked to metabolic complications such as insulin resistance, type 2 diabetes, and cardiovascular disease (Crewe et al., 2017; Rosen and Spiegelman, 2014). Despite extensive research, the causal processes promoting WAT inflammation in obesity remain unclear, although several initiating mechanisms have been proposed (Kammoun et al., 2014; Reilly and Saltiel, 2017).

Context and Significance

The adipose tissue of subjects with obesity displays a low-grade inflammation. While this negatively impacts tissue function, the mechanisms promoting inflammation are not well understood. Researchers at Karolinska Institutet and their collaborators asked whether changes in fat tissue metabolism may underly inflammation. By analyzing metabolites from human fat tissue samples, they discovered that the amino acid glutamine was the most markedly reduced factor in obese subjects. By combining studies in human cell cultures and in mice, they observed that glutamine rewired the metabolism of adipose tissue cells and lowered the expression of inflammatory genes. This was mediated via mechanisms involving the modification of proteins regulating gene expression. Altogether, glutamine may alleviate adipose inflammation and improve fat tissue function in obesity.

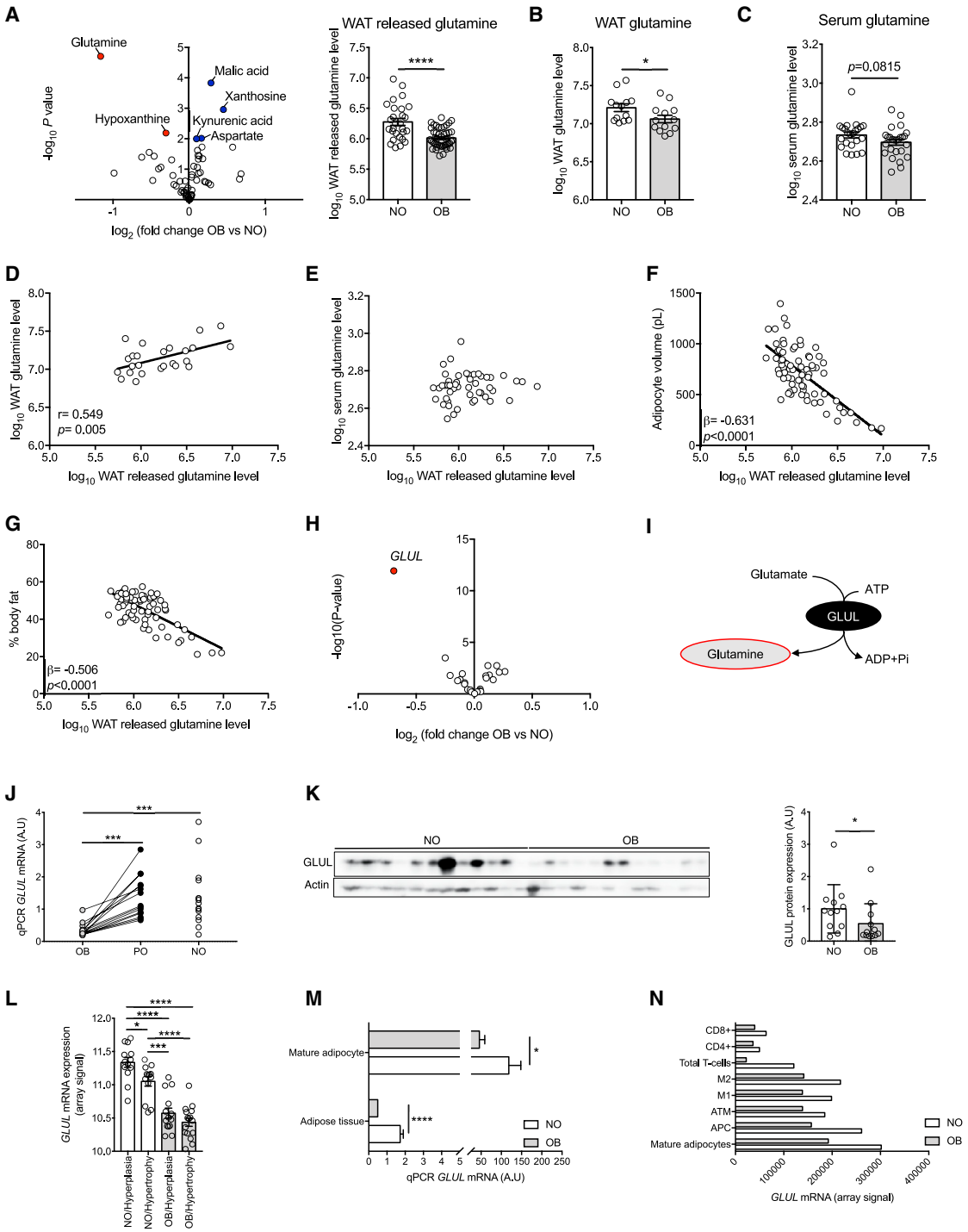

Figure 1. Reduced Glutamine Levels Are a Metabolic Signature of Obese White Adipose Tissue

(A) The release of polar metabolites from WAT in cohort 1 (n = 81) represented in a volcano plot with the fold change (log_2) expressed as the levels in obese (OB) versus never-obese (NO) subjects on the x axis and p values on the y axis (log_{10}). Significantly ($p < 0.01$) regulated metabolites marked in color: red are downregulated and blue upregulated in obesity (left panel). Levels of glutamine plotted in a bar chart with individual values in NO and OB subjects (right panel).

(B) Glutamine levels (log_{10}) in whole WAT comparing NO and OB individuals shown for a subgroup of cohort 1 (n = 26).

(C) Serum glutamine levels (log_{10}) compared between NO and OB individuals in cohort 1 (n = 53).

(D and E) Correlation between released WAT glutamine and WAT tissue glutamine (D) as well as serum glutamine levels (E).

(F and G) Multiple regression analysis between WAT-released glutamine and adipocyte volume (F) or percent body fat (G) was performed and corrected for BMI. p values and standardized beta coefficients are shown in the plots.

(legend continued on next page)

It is well established that the metabolic state of a cell impacts its transcriptional activity via intermediary metabolites that constitute substrates or co-substrates for enzymes modifying the chromatin and/or the activity of transcriptional regulators (Berger and Sassone-Corsi, 2016; Etchegaray and Mostoslavsky, 2016). To date, >100 types of post-translational modifications have been described and shown to be regulated by thousands of different metabolites (Reid et al., 2017). Several of these may modulate the epigenome; e.g., the balance between acetyl-coenzyme A and nicotinamide adenine dinucleotide levels regulates protein acetylation while O-linked β-N-acetylglucosamine (O-GlcNAc) modification is controlled by several intermediary metabolites including glucose, glutamine, acetyl-coenzyme A, and uridine (Etchegaray and Mostoslavsky, 2016). Findings over the last decades have demonstrated an intimate crosstalk between metabolism and the immune system (Lee et al., 2018) often referred to as "immunometabolism" (Mathis and Shoelson, 2011). For example, folate metabolism has recently been implicated in regulating the expression of pro-inflammatory and reducing pro-adipogenic pathways via epigenetic mechanisms in human adipocytes (Petrus et al., 2018a). Thus, changes in intracellular metabolites may influence chromatin organization and thereby the transcriptional fingerprint of adipocytes, further suggesting that certain metabolic states in WAT regulate inflammation via crosstalk between metabolism and the epigenome.

WAT releases a variety of polar and non-polar metabolites that act in an auto-, para-, or endocrine fashion. As WAT is mainly composed of lipids, there has been little focus on investigating the role of non-lipid/polar metabolites in this tissue (Kučera et al., 2018). We hypothesized that specific polar WAT metabolites could constitute causal factors linking obesity to WAT inflammation. To this end, we mapped the metabolome released from subcutaneous abdominal WAT of obese and non-obese individuals. Combined analyses in human and murine WAT as well as human adipocytes demonstrate that glutamine metabolism is disturbed in the obese state, which results in increased chromatin O-GlcNAcylation and expression of genes in pro-inflammatory pathways.

RESULTS

White Adipose Tissue from Obese Individuals Displays Lower Glutamine Levels

We set out to map the polar metabolome released from subcutaneous abdominal WAT *ex vivo* in a cohort of 52 obese and 29 non-obese women (cohort 1; clinical data in Table S1). This identified six metabolites that displayed highly significant ($p < 0.01$) differences between non-obese and obese subjects (Figure 1A; Table S2). Among these, glutamine displayed both the largest fold change and highest significance level and was therefore selected for more in-depth analyses. WAT lysates were available from a subset (n = 26) of the individuals in cohort 1; analyses confirmed that the glutamine levels were lower in the tissue of obese subjects (Figure 1B). In serum samples (n = 53), there was a slight but non-significant difference in glutamine levels between obese and non-obese individuals (Figure 1C). WAT-released glutamine levels correlated with the levels detected in WAT lysates (Figure 1D), but not with those measured in serum (Figure 1E), suggesting that glutamine levels in obesity were locally dysregulated in human WAT. Further analyses of WAT glutamine release showed an inverse, body mass index (BMI)-independent association with fat cell volume (Figure 1F) and body fat percent (%) (Figure 1G). These data demonstrate that attenuated glutamine levels in WAT associate with increased fat mass and fat cell size.

Adipose Tissue Is Characterized by Altered Expression of Glutamine-Metabolizing Genes in Obesity

The expression of genes encoding glutamine-regulating proteins (enzymes and transporters as described in Bhutia and Ganapathy, 2016; Yelamanchi et al., 2016; listed in Table S3) and their link to obesity was mapped using transcriptomic data from a previously described cohort (cohort 2, Table S1; Arner et al., 2012) consisting of 56 non-obese and obese women. Out of the 26 analyzed genes, 13 were significantly different between obese and non-obese subjects. The largest fold difference as well as highest significance was observed for *GLUL*, which was lower in the obese group (Figure 1H). *GLUL* encodes glutamine synthetase, which uses glutamate as a substrate and is the only known glutamine-synthesizing enzyme (Figure 1I). Further evidence supporting the notion that fat mass impacts *GLUL* expression was provided by analyzing WAT in obese women before and 2 years after bariatric surgery (termed post-obese, i.e., when they had reached a non-obese state) and never-obese controls (cohort 3, Table S1). This showed a normalization of *GLUL* after weight loss (Figure 1J). The low *GLUL* levels in the WAT of obese individuals were confirmed at the protein level (Figure 1K). Given the BMI-independent correlation between glutamine release and fat cell volume in Figure 1F, we subdivided subjects in cohort 2 according to fat cell morphology (hypertrophy/hyperplasia;

(H) The mRNA expression of glutamine-metabolizing genes from transcriptomics in WAT (cohort 2) of OB and NO represented in a volcano plot with *GLUL* marked in red.

(I) A cartoon representing the function of glutamine synthetase (GLUL).

(J) *GLUL* mRNA expression determined by qPCR in whole adipose tissue of obese women before (OB, n = 15) and after bariatric surgery (PO), and never-obese (NO, n = 15) controls matched for age and BMI with the subjects after bariatric surgery (cohort 3).

(K) Immunoblotting analysis of GLUL in whole WAT of NO and OB individuals (left panel) with the relative quantification of GLUL protein expression plotted in a bar chart displaying individual values (right panel).

(L) *GLUL* expression was compared between NO and OB individuals in cohort 2 subdivided according to fat cell morphology (hypertrophy/hyperplasia).

(M) qPCR analysis of *GLUL* gene expression in mature adipocytes and whole adipose tissue from NO and OB subjects.

(N) Expression of *GLUL* determined by gene microarray in various cell fractions of human subcutaneous WAT, including mature adipocytes, adipocyte progenitors (APC), adipose tissue macrophages (ATM as well as M1 and M2), and T cells (total, CD4+, and CD8+).

Student's t tests were performed for comparison between two groups and one-way ANOVA was performed for comparisons between several groups with Tukey's post hoc test. Correlation analysis was performed using Pearson's correlation coefficient or multiple regression analysis when correction for BMI was performed. Error bars are SEM. *$p < 0.05$, ***$p < 0.001$, ****$p < 0.0001$.

STAR Methods; Gao et al., 2014). Both obese and non-obese subjects with a pernicious hypertrophic phenotype displayed lower *GLUL* expression (Figure 1L). WAT is a heterogeneous organ consisting of several cell types, all of which contribute to metabolite release (Rosen and Spiegelman, 2014). The expression of *GLUL* in both isolated adipocytes and intact tissue was lower in obesity (Figure 1M). Analyses of microarray data from eight different WAT cell fractions (Acosta et al., 2017) showed that *GLUL* expression was highest in the adipocyte fraction, but that the levels were lower in all cell types in obesity (Figure 1N). Altogether, this suggests that the difference in WAT glutamine release between obese and non-obese subjects is driven by glutamine synthetase levels.

Low Glutamine Synthetase Expression Associates with Pro-inflammatory Pathways in Human Adipose Tissue

To gain insight into the role of glutamine in WAT, a gene ontology analysis was performed on genes associated with *GLUL* expression. This showed that *GLUL* was positively linked to genes in biological processes of lipid and carbohydrate metabolism, but inversely correlated with inflammatory processes and tissue remodeling (Figure 2A; Table S4). The association to inflammation was confirmed at the protein level as *GLUL* correlated negatively with the secretion of the established pro-inflammatory cyto- and chemokines (Donath and Shoelson, 2011; Kraakman et al., 2015; Weisberg et al., 2003), C-C chemokine ligand 2 (CCL2) (Figure 2B), interleukin 6 (IL6) (Figure 2C), and tumor necrosis factor alpha (TNFα) (Figure 2D). For IL6 and CCL2, the associations were BMI independent in multiple regression analyses.

Glutamine Attenuates Pro-inflammatory Pathways in Murine Adipose Tissue

To assess whether glutamine could affect WAT inflammation *in vivo*, male C57BL/6 mice were injected daily intraperitoneally with glutamine for 2 weeks (Figure 2E) followed by expression analysis of pro-inflammatory genes in epididymal WAT (eWAT; Figure 2F). In these non-obese animals on chow diet (CD), glutamine did not affect body weight (Figure S1A), food intake (Figure S1B), body composition and fat distribution (Figures S1C–S1G), fasting glucose levels (Figure S1H), or fat cell size (Figures S1I–S1K). Glutamine-treated animals displayed no significant change in *Glul* expression compared to littermates injected with PBS. However, the mRNA levels of pro-inflammatory markers including *Ccl2*, *Cd68*, and *Emr1* (encoding the macrophage marker EGF-like module-containing mucin-like hormone receptor-like 1; F4/80) were decreased (*Il1b*, *Il6*, and *Tnfa* were below the detection limit), while that of *Adipoq*, encoding the anti-inflammatory adipokine adiponectin, was increased (Figure 2F). Moreover, an inverse association between *Glul* and pro-inflammatory gene expression was evident in murine WAT of PBS-treated mice (Figure S1L). In contrast, this was not observed in the glutamine-treated group (Figure S1M), suggesting that exogenous glutamine supplementation may override the effect of endogenous *Glul*.

The effects of glutamine under conditions with increased inflammation were assessed in mice fed a high-fat diet (HFD) for 5 weeks where glutamine or PBS was injected during the final 2 weeks of HFD (Figure 2G). Chow-fed mice injected with PBS were used as a control for the effects of HFD. These time points were chosen based on qPCR analyses of eWAT samples from a previous study (Morgantini et al., 2019) showing that *Glul* expression was downregulated and inflammation was upregulated in mice on HFD compared with CD already after 3 weeks (see also STAR Methods; graph not shown). As expected, HFD led to a significant increase in body weight (Figure S2A; with a slight dip in connection with the glucose tolerance tests at day 11) and fat mass (Figures S2B–S2D), without alterations in lean body (Figure S2E) or liver mass (Figure S2F), and with no differences in food intake (Figure S2G), energy expenditure (Figure S2H), or respiratory exchange ratio (Figure S2I) between the two HFD groups. However, the proportional (%) increase in body weight (Figure S2J) and delta fat (Figure S2K), but not delta lean mass (Figure S2L), was attenuated in HFD-fed mice treated with glutamine compared to PBS. A reduction in fasting glucose (Figure S2M), insulin (Figure S2N), HOMA-IR (Figure S2O), and fat cell size (Figures S2Q–S2S) was also observed, while the effects on glucose tolerance were not significantly different between HFD mice on PBS or glutamine (Figure S2P). Our results are in line with longer ($\geq$8 weeks) glutamine treatments that have demonstrated reductions in WAT mass and hyperglycemia/-insulinemia in rodent HFD models (Abboud et al., 2019; Opara et al., 1996; Discussion). Gene expression analyses of eWAT confirmed that HFD increased the expression of all analyzed pro-inflammatory genes, which was attenuated in animals injected with glutamine (Figure 2H). In concordance, F4/80 immunohistofluorescence of eWAT showed a similar pattern (Figures 2I–2K), and flow cytometry confirmed that the proportion of pro-inflammatory macrophages (CD11c+) was normalized in glutamine-treated mice (Figure 2L; flow cytometry protocol detailed in Figure S2T).

High Glutamine Levels Attenuate Inflammation in Human Adipocytes and Leukocytes

There are well-established links between glutamine metabolism and reprogramming of T cells and macrophages (Araujo et al., 2017; Johnson et al., 2018; Klysz et al., 2015; Liu et al., 2017). However, the effects of glutamine on human adipocytes have not been studied. Hence, we incubated human *in vitro* differentiated adipocytes (STAR Methods) with various levels of glutamine throughout the 11-day-long differentiation. The glutamine concentrations ranged from 0.5 to 20 mM, where 2 mM is the standard concentration commonly used in cell culture media and 0.5 mM corresponds to the physiological plasma levels in humans (Figure 1C; Frayn et al., 1991), although 6–7 mM can be detected in critically ill subjects and 1–5 mM after glutamine supplementation in man (Berg et al., 2005). qPCR analyses showed that the expression of *CCL2*, *IL1B*, and *IL6* (*TNFA* was below the detection limit in these cell cultures) was attenuated by glutamine in a concentration-dependent manner with maximum effects observed at 5–20 mM (Figures 3A–3C). Further assessments of the time-induced effects were performed using 0.5 mM (low, L) or 10 mM (high, H) glutamine in the incubation medium. This showed that mRNA levels of *CCL2*, *IL1B*, and *IL6* were significantly attenuated at day 11 post-adipogenic induction (Figures 3D–3F). Consequently, these concentrations and the 11-day incubation time were chosen for all subsequent analyses. While high glutamine did not affect the number of lipid-containing cells (Figure S3A) or the gene expression of adipocyte-specific genes (Figure S3B), it reduced lipid content

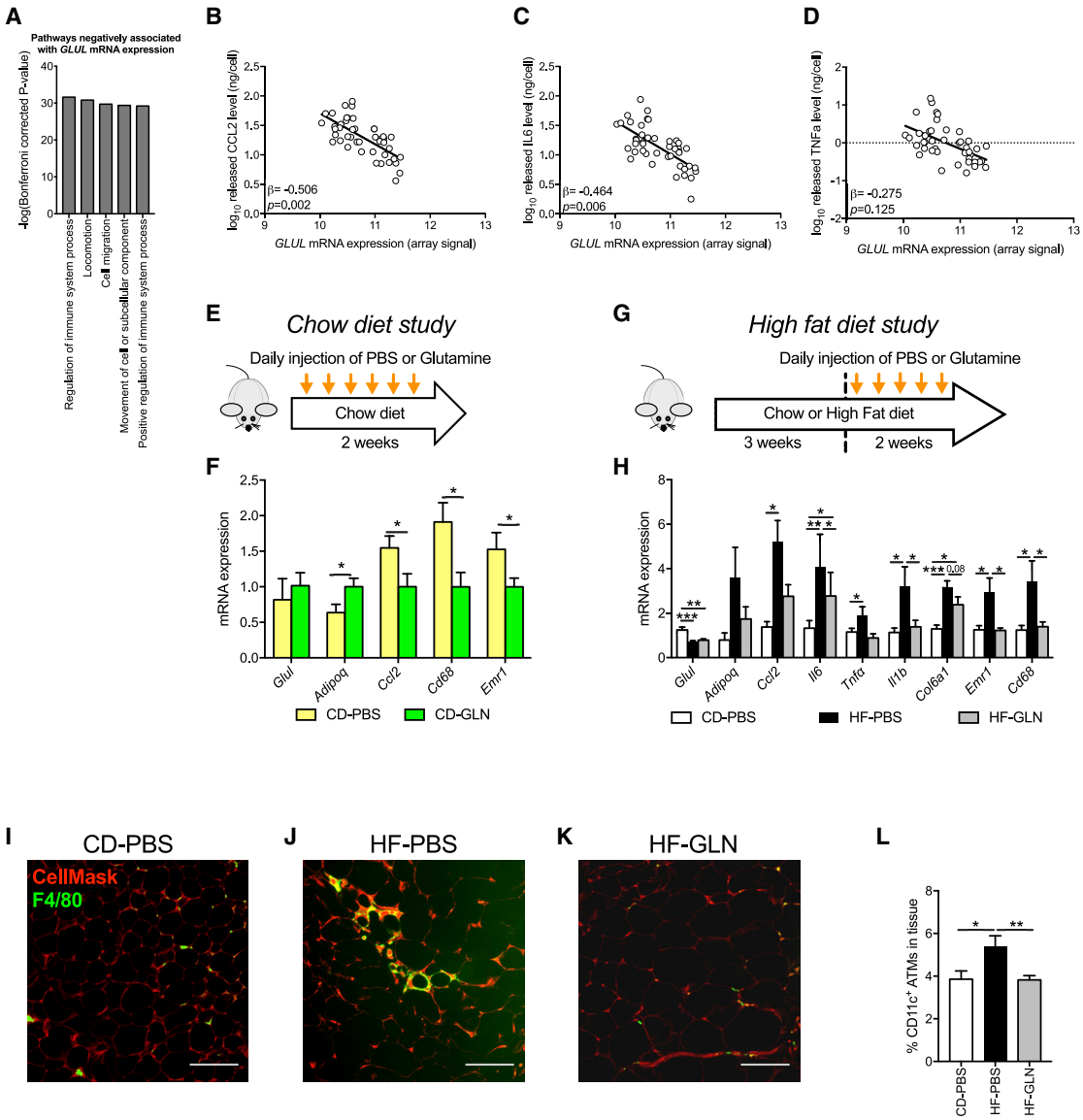

Figure 2. Glutamine Regulates Inflammation in White Adipose Tissue

(A) Gene ontology (GO) analysis of genes negatively associated with *GLUL* mRNA expression.

(B–D) Multiple regression analyses of the correlation between *GLUL* mRNA expression and *ex vivo* WAT-released CCL2 (B), IL6 (C), and TNFα (D) (cohort 2). BMI was included as an independent regressor and standardized beta coefficients and p values are shown in the graphs after BMI correction.

(E) A cartoon detailing the glutamine administration intervention in mice fed a chow diet. Mice were injected intraperitoneally with glutamine (1 g/kg body weight) or PBS (20 mL/kg body weight) daily for 2 weeks. After sacrifice, epigonadal WAT (eWAT) samples were isolated for gene expression analyses by qPCR.

(F) Gene expression in eWAT from chow-fed animals treated with PBS or glutamine as indicated in (E).

(G) A cartoon representing the glutamine administration intervention in mice fed chow or a high-fat (HF) diet.

(H) Gene expression in eWAT from animals in the intervention illustrated in (G); chow- (CD-PBS) or HF diet-fed animals injected with either PBS (HF-PBS) or glutamine (HF-GLN).

(I–K) Representative microphotographs of eWAT from the three groups in (G) stained for the macrophage marker F4/80 (green) and CellMask (red). Scale bar, 100 μm.

(L) Proportion of CD11c-positive cells by flow cytometry in eWAT stromal vascular fractions obtained from the mice illustrated in (G).

In (F), (G), and (L), Student's t test was used for comparisons between groups and significant differences are indicated. Error bars are SEM. *p < 0.05, **p < 0.01, ***p < 0.001.

per cell (i.e., lipid droplet area and intensity; Figure S3A). Global transcriptomic analysis confirmed the anti-inflammatory effects in cells incubated in high concentrations of glutamine (Figure S3C; Table S5) and were validated at the protein level (Figures 3G–3I). Additional experiments were performed where *in vitro* differentiated adipocytes incubated in low or high glutamine for 11 days were then switched to high and low glutamine levels, respectively (Figures 3J–3L). This showed that a switch

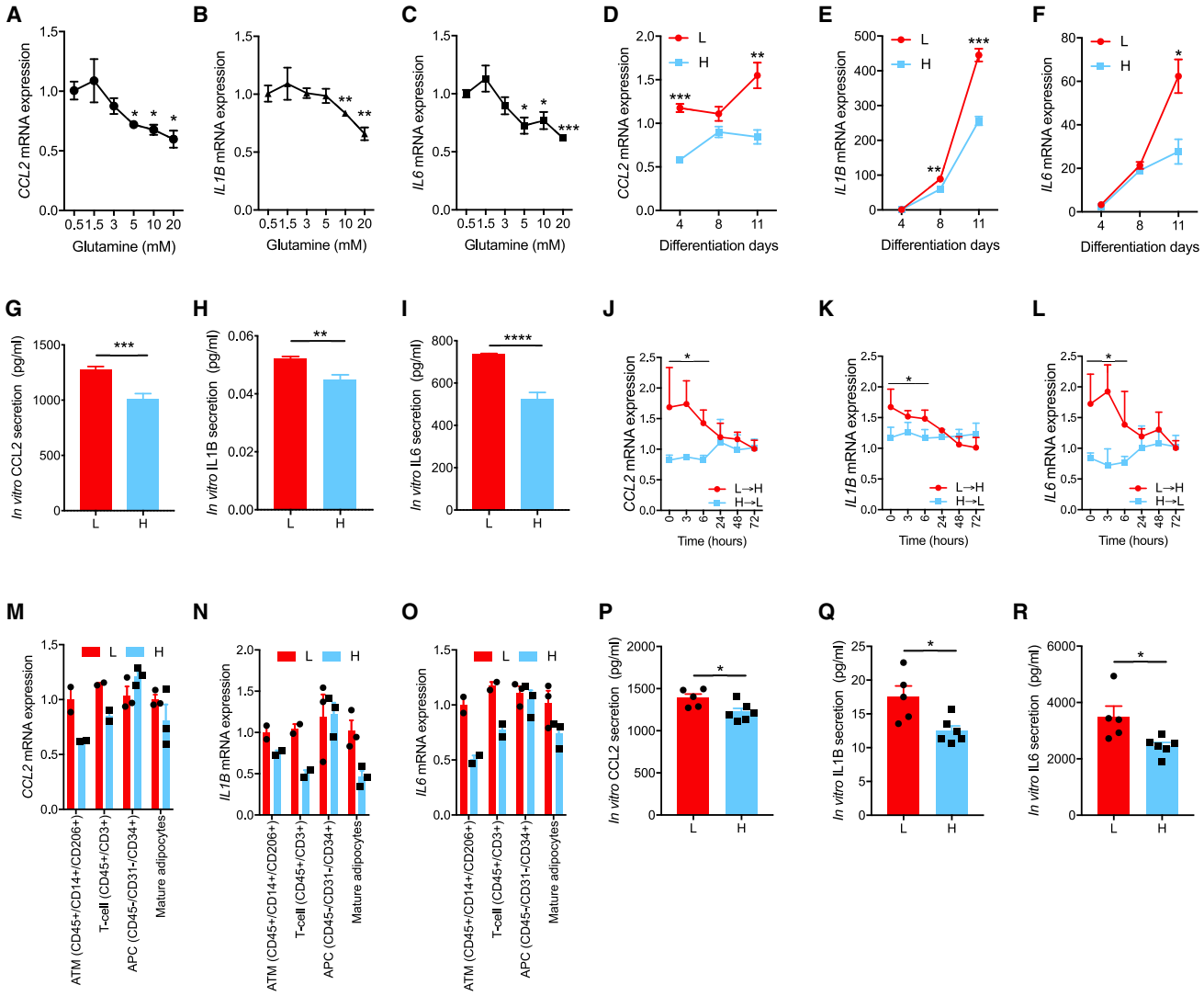

Figure 3. Glutamine Attenuates Pro-inflammatory Adipokine Levels in Mature Adipocytes, but Not Progenitors

(A–C) qPCR analysis of *CCL2* (A), *IL1B* (B), and *IL6* (C) in *in vitro* differentiated human adipocytes incubated with glutamine concentrations ranging from 0.5 to 20 mM.

(D–F) qPCR analysis of *CCL2* (D), *IL1B* (E), and *IL6* (F) expression in *in vitro* cultured human adipocytes incubated with high (H, 10 mM) or low (L, 0.5 mM) glutamine analyzed at three time points post-adipogenic induction.

(G–I) The protein release of CCL2 (G), IL1B (H), and IL6 (I) at day 11 of differentiation in cells incubated with high (H) or low (L) glutamine levels.

(J–L) qPCR analysis of *CCL2* (J), *IL1B* (K), and *IL6* (L) assessed in *in vitro* differentiated adipocytes switching from high to low (H→L) or low to high (L→H) glutamine concentrations at day 11 of differentiation.

(M–O) The expression of *CCL2* (M), *IL1B* (N), and *IL6* (O) expression in various cell types extracted from human adipose tissue and incubated in culture media with high (H) or low (L) glutamine for 48 h. ATM, adipose tissue macrophages defined as CD45+/CD14+/CD206+ cells; T cells defined as CD45+/CD3+ cells; APC, adipocyte progenitors defined as CD45−/CD31−/CD34+ cells and mature adipocytes. In the qPCR, *PPIA* was used as reference gene for ATM, T cells, and APC while *LRP10* was used for mature adipocytes (see also STAR Methods for details).

(P–R) The protein release of CCL2 (P), IL1B (Q), and IL6 (R) from mature adipocytes incubated in culture media with high (H) or low (L) glutamine for 48 h.

Student's t test was used for comparison between groups. Error bars are SEM. *p < 0.05, **p < 0.01, ***p < 0.001, ****p < 0.0001.

from low to high glutamine attenuated the mRNA levels of pro-inflammatory genes within 6 h. All experiments above were performed under normal culture conditions when the endogenous expression of pro-inflammatory cyto- and chemokines is relatively low. To evaluate the effect of glutamine under stimulated conditions, adipocytes were cultured in high or low glutamine for 11 days followed by a 3 h incubation with TNFα. This resulted in a marked upregulation of *CCL2*, *IL1B*, and *IL6*, a response that was significantly attenuated (by 30%–50%) in cells incubated with high glutamine (Figure S3D). Together with the *in vivo* data in CD- and HFD-fed mice, this suggests that the anti-inflammatory effects of glutamine are present under a wide range of conditions. These studies were performed in *in vitro* differentiated adipocytes, which may differ from mature adipocytes *in vivo*, and WAT is composed of additional cell types. We therefore also isolated primary cells from human

WAT and determined the effects of high or low glutamine incubations for 48 h (Figures 3M–3O). Incubations with high glutamine resulted in anti-inflammatory effects in macrophages, T cells, and mature adipocytes, where the latter was also demonstrated at the protein level (Figures 3P–3R). In contrast, there was no detectable effect in adipocyte progenitors (Figures 3M–3O). Altogether, our data confirm that glutamine exerts anti-inflammatory effects on macrophages and T cells and extends this to include differentiated adipocytes as well as WAT *in vivo*.

High Glutamine Levels Attenuate Glycolysis in Adipocytes

Glutamine is a source of energy that fuels the citric acid cycle by conversion to glutamate and then α-ketoglutarate. In immune cells, glutamine has been suggested to affect cell phenotype by shifting energy substrate utilization from glycolysis to glutaminolysis (Araujo et al., 2017; Ren et al., 2019). These regulatory effects have partly been attributed to changes in the levels of intermediary metabolites resulting in chromatin remodeling and altered gene transcription (Johnson et al., 2018; Liu et al., 2017). Hence, we hypothesized that glutamine may induce anti-inflammatory effects in human adipocytes by altering intracellular metabolism. Bioenergetics analyses showed reduced glycolytic rates in cells treated with high glutamine as the extracellular acidification rate (ECAR) was reduced in relation to the oxygen consumption rate (OCR) (Figures 4A–4C). In accordance, the cells were more efficient in utilizing glutamine as an energy source (Figure 4D). Additionally, they displayed lower glycolytic capacity in response to glucose (Figure 4E) as well as reduced glucose uptake (Figure 4F). That decreased glycolysis could affect pro-inflammatory gene expression was further suggested by the glucose-dependent increase in *IL1B* and *IL6* mRNA expression in adipocytes, which was attenuated by increasing glutamine concentrations (Figures 4G–4I). Moreover, a 24 h-long treatment with the glycolysis inhibitor 2-deoxyglucose (2DG, a competitive inhibitor of hexokinases; Figure S4A) attenuated glycolysis (Figure 4J) and lowered both gene expression and protein secretion of CCL2, IL1B, and IL6 in cells incubated with low (but not high) glutamine (Figures 4K–4P). Glycolysis is a multistep pathway that converts glucose into pyruvate, but with additional branching into the pentose phosphate and the hexosamine biosynthetic pathway (HBP) after the conversion of glucose-6-phosphate or fructose-6-phosphate, respectively (Figure S4A). To tease out whether inhibition of glycolysis before or after these branches was of importance, genes involved in early and late stages of the glycolytic pathway were knocked down. Hexokinase 1 and 2 (encoded by *HK1* and *HK2*, respectively) are the two enzymes that catalyze the first step of glycolysis where the expression of *HK2* is markedly induced during adipogenesis (Figure S4B). Upon *HK2* knockdown by RNAi (Figure S4C), similar effects as with 2DG were observed on ECAR (Figure S4D) as well as on *IL1B* and *IL6* expression, particularly in the low glutamine condition (Figures S4E–S4G). In contrast, a reduction in the expression of inflammatory factors was not observed when knocking down *ENO1*, encoding Enolase 1, an enzyme further down in the glycolytic pathway (downstream of the HBP; Figures S4H–S4K). This establishes a link between altered glycolysis activity and inflammation where early steps prior to the HBP appear to be involved.

Metabolomics Link Low Glutamine to Nuclear Protein O-GlcNAcylation

The effects on glycolysis suggested that glutamine re-wired metabolism and that the resulting changes in intracellular metabolites could be involved in the transcriptional control of genes involved in inflammation. More detailed information on the regulation of specific metabolites was obtained by untargeted metabolomics analyses of cells incubated in either high or low glutamine concentrations. This confirmed that high glutamine reduced the levels of key metabolites in glycolysis, e.g., glucose-6-phosphate, 3-phosphoglycerol, and phosphoenolpyruvate (Figure S4A). Furthermore, glutamine *in vitro* impacted to a proportionally higher degree the levels of polar metabolites, particularly those in amino acid and carbohydrate metabolism (Figure 5A; Table S6). To gain insights into the possible physiological relevance of the glutamine-induced effects on intracellular metabolites, the data were compared with metabolomics performed in WAT samples from the sub-group of cohort 1 (n = 26). In WAT samples there was no enrichment for any specific polar metabolite group in obesity (Figure 5B; Table S6). The polar metabolites concordantly altered both *in vivo* and *in vitro* (i.e., differentially regulated between obese and non-obese subjects as well as low and high glutamine incubation) were few. Notably, in contrast to what has been reported in immune cells, tricarboxylic acid cycle metabolites (e.g., α-ketoglutarate) were not among these. Instead, they included, apart from glutamine itself (Figure 5C), sedoheptulose-7-phosphate, UDP-N-acetylglucosamine/galactosamine (UDP-GlcNAc), 5-galactosylhydroxy-L-lysine, N-acetylglutamate, and uridine (Figures 5D–5F). Among these, UDP-GlcNAc is synthesized within the HBP and several metabolites in this pathway were lower in cells incubated with high glutamine (Figure S4A). UDP-GlcNAc is the only substrate for the enzyme O-GlcNAc transferase (OGT), which catalyzes the post-translational modification O-GlcNAc on serine or threonine residues (Yang and Qian, 2017). O-GlcNAcylation impacts several aspects of protein function and chromatin remodeling (Etchegaray and Mostoslavsky, 2016) and has been implicated in the regulation of inflammation in a murine adipocyte cell line (Wollaston-Hayden et al., 2015). Protein O-GlcNAcylation can occur both in the nucleus and in the cytosol (Yang and Qian, 2017). We therefore performed O-GlcNAc quantification both in the nuclear and cytosolic fraction of human adipocytes treated with high and low glutamine. This showed that incubation with high glutamine attenuated O-GlcNAcylation in the nucleus in a concentration- and glucose-dependent manner (Figure 6A). In contrast, no changes were observed in the cytosol (Figure S5A). In concordance with the *in vitro* data, global O-GlcNAcylation was higher in WAT of obese individuals (Figure 6B) and lower in mice injected with glutamine either on chow (Figure 6C) or HFD (Figure 6D). Taken together, these data suggest that the attenuating effect of glutamine on glycolysis reduces the levels of HBP metabolites including UDP-GlcNAc and thereby O-GlcNAcylation.

Glutamine Regulates IL6 and IL1B, but Not CCL2, via O-GlcNAcylation

We hypothesized that glutamine mediates at least part of its anti-inflammatory effects via reduction of nuclear protein O-GlcNAcylation. To demonstrate a causal link, *OGT* was

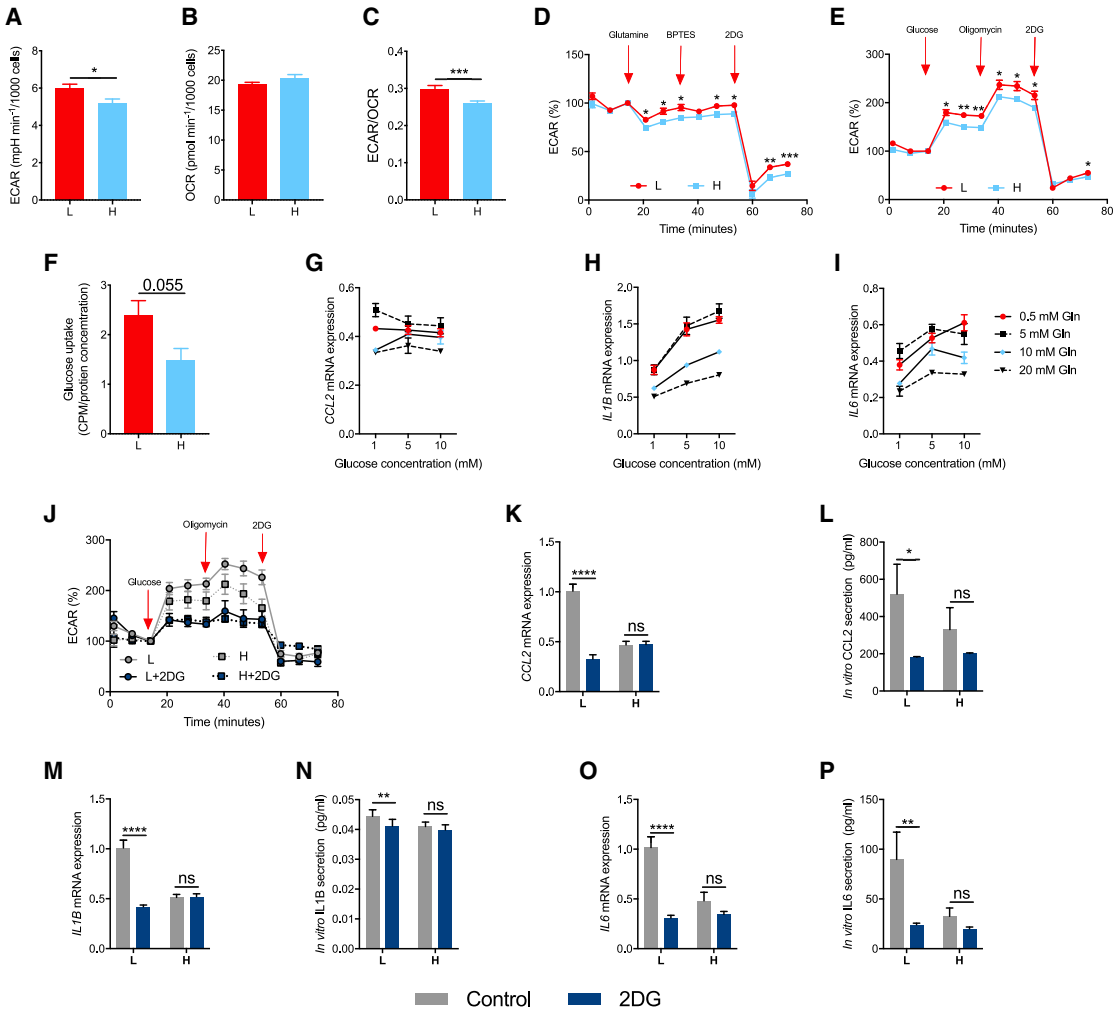

Figure 4. Glutamine Attenuates Inflammation via Reduced Glycolysis

(A–C) The basal glycolytic rate expressed as extracellular acidification rate (ECAR) (A) and oxidative rate expressed as oxygen consumption rate (OCR) (B) and the ratio (C) in *in vitro* differentiated human adipocytes incubated with high (H, 10 mM) or low (L, 0.5 mM) glutamine for 11 days.

(D and E) The metabolic flexibility in response to glutamine (D) and glucose (E) in *in vitro* differentiated human adipocytes incubated with high (H) or low (L) glutamine levels.

(F) Glucose uptake level in *in vitro* differentiated human adipocytes incubated with high (H) or low (L) glutamine concentrations.

(G–I) Gene expression of *CCL2* (G), *IL1B* (H), and *IL6* (I) in cells incubated with various combinations of glucose (1–10 mM) and glutamine (0.5–20 mM) concentrations.

(J) The metabolic flexibility in response to glucose in human adipocytes incubated with high (H) or low (L) glutamine levels with (0.1 mM) or without (control is vehicle, water) the competitive glycolysis inhibitor 2-deoxyglucose (2DG) for 24 h.

(K–P) Gene expression and protein secretion of CCL2 (K and L), IL1B (M and N), and IL6 (O and P) in cells treated with high or low glutamine with or without 2DG. Student's t test was used for comparison between groups. ns, non-significant. Error bars are SEM. *p < 0.05, **p < 0.01, ***p < 0.001, ****p < 0.0001.

knocked down using small interfering RNA (siRNA) in human adipocytes incubated with high or low glutamine. This resulted in a significant downregulation of both OGT gene and protein expression (Figures S6A and S6B). As expected, the knockdown conferred a reduction in global O-GlcNAcylation in nuclear lysates (Figure S6B). In agreement with data in Figure 3, high glutamine reduced the gene and protein expression of the measured pro-inflammatory factors (Figures 6E–6J). The mRNA expression as well as protein secretion of IL1B and IL6 under low glutamine conditions was significantly reduced by *OGT* knockdown (Figures 6G–6J). In contrast, CCL2 mRNA was not influenced (Figure 6E) and the secretion levels even slightly increased (Figure 6F). Moreover, inhibition of OGT activity by GalNAc-*O*-bn for 24 h phenocopied the effects observed in cells incubated with low glutamine after *OGT* knockdown (Figures S6C–S6I). Conversely, a 24 h-long incubation with PUGNAc (an inhibitor of OGA, the enzyme that removes O-GlcNAc molecules from proteins) increased O-GlcNAcylation (Figure S6C) as well as IL1B and IL6 expression/secretion in cells incubated with high glutamine (Figures 6K–6P). Similar to the findings with *siOGT* and GalNAc-*O*-bn, the effects of PUGNAc on CCL2 expression/secretion did not support a role for O-GlcNAcylation

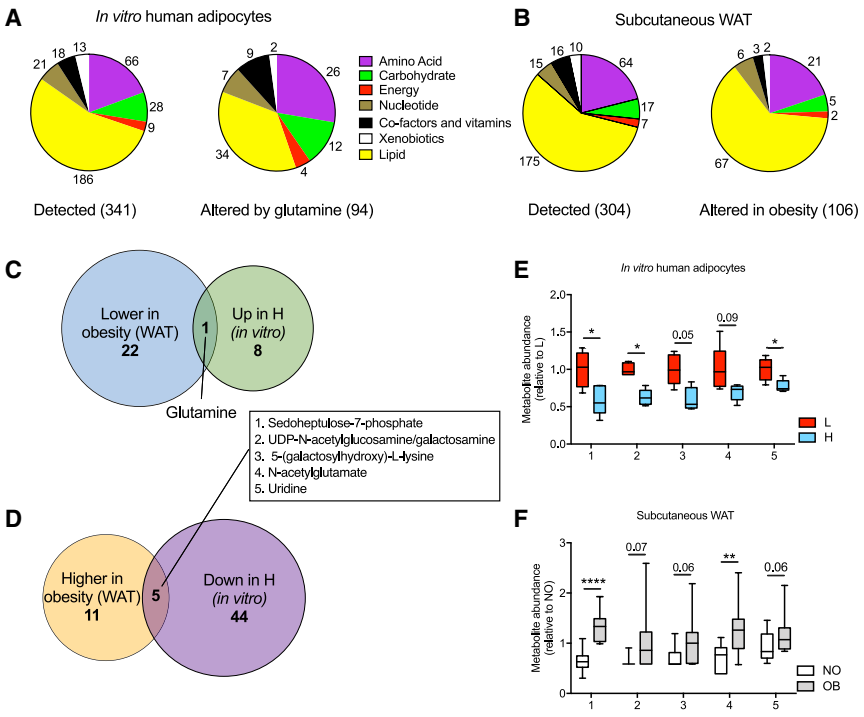

Figure 5. Global Metabolomics Analyses in *In Vitro* Differentiated Adipocytes and White Adipose Tissue

(A) The relative proportion of metabolite groups detected in *in vitro* differentiated human adipocytes (left panel) and the ones differentially regulated in cells incubated with high and low glutamine (right panel).

(B) The relative proportion of metabolite groups detected in subcutaneous WAT (left panel) and the ones significantly different between obese (OB) and non-obese (NO) (right panel) (subgroup of cohort 1, n = 26).

In (A) and (B), numbers refer to the number of metabolites.

(C and D) The overlap between the significantly ($p < 0.10$) regulated metabolites that were lower in WAT from obese individuals and (reciprocally) upregulated by high glutamine (C) or higher in obese subjects and downregulated by high glutamine *in vitro* (D).

(E and F) The five metabolites overlapping in (D) depicted in box plots (min-max) in human adipocytes incubated with high and low glutamine (E) and WAT of OB and NO subjects (F).

Comparison of two groups was performed with Welch's two-sample t test. *$p < 0.05$, **$p < 0.01$, ****$p < 0.0001$.

in the regulation of this chemokine. We also confirmed that attenuating glycolysis using 2-deoxyglucose (Figure S6J) reduced O-GlcNAcylation (Figure S6K). Together with the data on RNAi targeting glycolytic enzyme enzymes up- or downstream of the HBP branching (Figure S4), these results support the notion that glutamine attenuates the expression of specific pro-inflammatory genes via O-GlcNAcylation.

Characterization of the O-GlcNAcylated Proteome and Its Spatial Localization on the Chromatin

While O-GlcNAcylation plays a fundamental role in cell biology (Yang and Qian, 2017), little is known regarding its role in white adipocytes. To characterize the human adipocyte O-GlcNAcylated proteome and its possible involvement in transcriptional regulation, nuclear proteins were immunoprecipitated using a pan-O-GlcNAc antibody followed by untargeted proteomics (STAR Methods). This identified >400 proteins that could be grouped into six main clusters of protein interactomes assigned to biological processes involved in RNA processing, ribosome biogenesis and protein transport, cellular structure, and chromatin organization and epigenetic processes (Figure 7A; Table S7). In addition, a set of previously described transcriptional regulators important for adipocyte function were identified (e.g., SP1 and EBF1; Gao et al., 2014; Kulyté et al., 2014).

Proteins involved in chromatin organization, RNA splicing, and gene transcription mediate their effects by proximal binding, directly or indirectly, to the chromatin. Hence, the O-GlcNAcylated proteome was mapped along the genome by chromatin immunoprecipitation followed by DNA sequencing (ChIP-seq) in *in vitro* differentiated human adipocytes incubated with low or high glutamine. In agreement with findings in Figure 6A, overall chromatin O-GlcNAcylation levels were lower in adipocytes incubated with high glutamine (Figures 7B and 7C; Table S7). Furthermore, a pathway analysis confirmed that glutamine attenuated O-GlcNAcylation in the vicinity of genes in pro-inflammatory pathways (Figure S7A). To determine the contribution of each O-GlcNAcylated protein to the differentially O-GlcNAcylated regions on the chromatin would require ChIP-seq analyses of each of the >400 proteins detected in the proteomic analysis, which was out of the scope of the present study. Nevertheless, a motif binding analysis of the differentially O-GlcNAcylated regions allowed us to map possible transcription factors for which the activity could be influenced by O-GlcNAcylation (Figure 7D). Among the identified transcription factor motifs, only SP1 was found to be directly O-GlcNAcylated in the proteomic analysis (Figure 7A; Table S7). In protein lysates from adipocytes incubated with high or low glutamine, immunoprecipitation using a pan-O-GlcNAc antibody followed by detection with an anti-SP1 antibody revealed lower SP1 O-GlcNAcylation under high glutamine conditions (Figure 7E).

A 24 h incubation with mithramycin A, a selective inhibitor of SP1, repressed *IL1B* and *IL6* expression in cells incubated with low and high glutamine levels (Figure 7F). However, analysis of the ChIP-seq data revealed that O-GlcNAc-modified proteins did not interact with *IL1B* or *IL6* gene promoters (tracks not shown), suggesting that SP1 and O-GlcNAc modification may regulate the expression of these genes by affecting other regions on the chromatin. To obtain insights into the primary gene targets of the glutamine-O-GlcNAcylation-SP1 pathway in human adipocytes, we performed a ChIP-seq of SP1 to identify genes with at least one SP1 peak call in the promoter as well as gene expression microarray following SP1 RNAi to define the SP1-regulated transcriptome (STAR Methods). These data were overlapped with the genes (1) regulated by glutamine (Table S5) and (2) displaying reduced O-GlcNAcylation after glutamine treatment (Figure S7B; Table S7; STAR Methods). This resulted in a

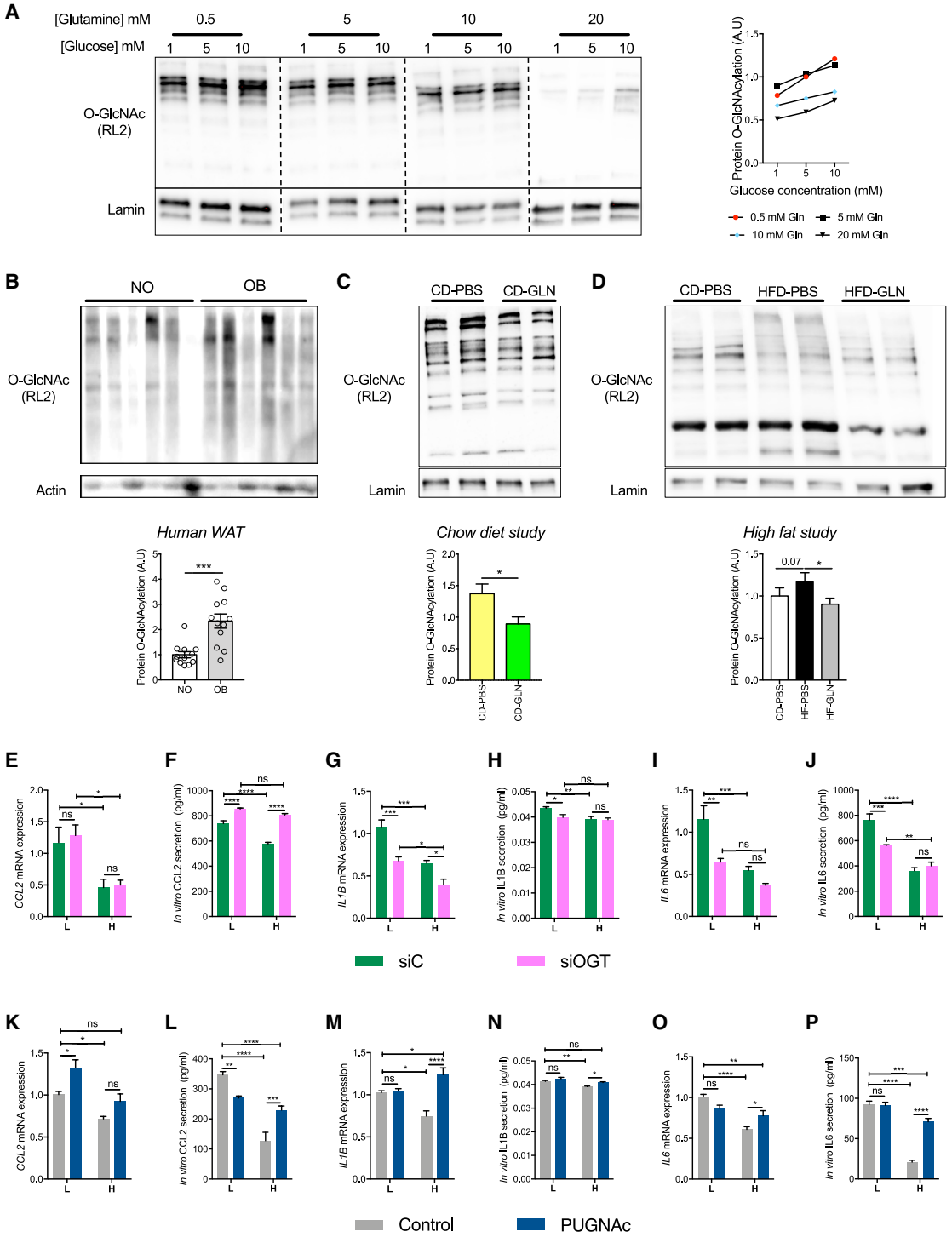

Figure 6. Glutamine Regulates Inflammation via Protein O-GlcNAcylation

(A–D) Western blots of global protein O-GlcNAcylation in (A) adipocyte nuclei isolated from *in vitro* differentiated adipocytes incubated with various combinations of glutamine and glucose, (B) whole WAT from never-obese (NO) and obese (OB) subjects, (C) eWAT from chow-fed mice treated with PBS (CD-PBS) or glutamine (CD-GLN), and (D) mice on chow (CD-PBS) or high-fat (HF) diet treated with PBS (HF-PBS) or glutamine (HF-GLN). The corresponding quantifications of the western blots are shown.

(E–P) Gene expression and protein release of CCL2 (E, F, K, and L), IL1B (G, H, M, and N), and IL6 (I, J, O, and P) from *in vitro* differentiated adipocytes treated with high (H) or low (L) glutamine in combination with siRNA targeting *OGT* (E–J) or the OGA inhibitor PUGNAc (the latter at 0.2 mM for 24 h, control is vehicle, DMSO)

(legend continued on next page)

list of 69 genes out of which 43 appeared at least once together with the search term "inflammation" in PubMed (Table S7). Among these, three genes (*ETS1*, *RICTOR*, and *PFKFB3*) were selected for further validation. Track analyses of the ChIP-seq data in the promoter regions (up to 5 kb upstream of the transcription start site) revealed differentially O-GlcNAcylated peaks under low and high glutamine conditions that overlapped with SP1 binding sites (Figure S7C). ChIP-qPCR using antibodies directed against O-GlcNAc or SP1 (the latter using two independent antibodies) confirmed glutamine-regulated O-GlcNAcylation as well as SP1 binding in the corresponding regions (Figures S7D–S7F). Finally, incubations with glutamine, mithramycin A, or PUGNAc demonstrated that all three genes were regulated by glutamine, SP1, and O-GlcNAcylation (Figures S7G–S7I). This suggests that the glutamine-induced changes in the expression of inflammation-linked genes via attenuated O-GlcNAcylation involve at least in part specific SP1 targets (Figure 7G).

DISCUSSION

Herein, we report glutamine to be an immunometabolic regulator in WAT that links obesity to inflammation. At least in adipocytes, reduced glutamine levels result in increased UDP-GlcNAc levels and O-GlcNAcylation of chromatin-binding proteins located near inflammatory genes. Our results in adipocytes combined with previous data on glutamine metabolism in macrophages and T cells (Araujo et al., 2017; Johnson et al., 2018; Liu et al., 2017; Ren et al., 2019) support a model wherein the metabolic micro-environment impacts WAT function through a coordinated effect on several cell types.

Most studies using metabolomics to compare lean and obese subjects have focused on analyses of plasma/serum or lipidomics in small sample numbers of WAT (Cirulli et al., 2019; Kučera et al., 2018). We were interested in analyzing polar metabolites acting locally in the microenvironment of WAT that may influence its phenotype. Secretion of purine metabolites from WAT has recently been studied in a targeted manner in samples from four lean subjects (Nagao et al., 2018). In concordance with that study, we found both hypoxanthine and xanthosine to be released from WAT. In addition, they were differentially regulated between obese and non-obese individuals (Figure 1A). In our cohort of 81 non-obese and obese individuals, the difference in glutamine release was the most prominent between the two conditions and was (in contrast to the other differentially regulated metabolites) associated with body fat percentage and fat cell volume independently of BMI. Glutamine is conditionally essential and the most abundant amino acid in the body (Frayn et al., 1991). It participates in central metabolic processes by acting as an energy substrate for the tricarboxylic acid cycle and a nitrogen donor in several pathways including purine/pyrimidine synthesis, nicotinamide adenine dinucleotide metabolism, and the urea cycle (Yelamanchi et al., 2016). The clinical potential of glutamine has been studied in a plethora of conditions ranging from critical illness (Cruzat et al., 2018) to the metabolic syndrome (Laviano et al., 2014) and type 2 diabetes (Mansour et al., 2015). Even a single dose has been reported to have measurable physiological effects, e.g., on GLP-1 and insulin secretion (Meek et al., 2015). Furthermore, in murine models of diet-induced obesity, long-term supplementation with glutamine improved glucose metabolism (Cheng et al., 2012; Opara et al., 1996), but resulted also in body-weight reduction (Opara et al., 1996), making it difficult to define the primary mechanisms.

A link between circulating levels of glutamine, body weight, and metabolic health is supported by independent findings showing that low glutamine levels predict incident type 2 diabetes in large population-based cohorts (Cheng et al., 2012). In our discovery cohort (cohort 1), there was no correlation between WAT glutamine release and the serum levels. This is most probably explained by the fact that WAT is a minor net contributor to plasma glutamine compared with skeletal muscle (Frayn et al., 1991). In addition, in our study WAT biopsies were taken after an overnight fast, which has been shown to induce glutamine synthetase levels in muscle (Kinouchi et al., 2018). Thus, we cannot exclude that our experimental design may have masked a more significant contribution of WAT-derived glutamine to the circulation. Nevertheless, the obesity-induced changes in local glutamine levels prompted us to investigate the expression of genes involved in glutamine metabolism and transport in WAT. Transcriptomic analyses showed that *GLUL* was the most prominently dysregulated gene in the glutamine pathway in obesity. Although the gene expression levels were higher in the adipocyte fraction, all cell types of WAT expressed *GLUL* and displayed lower levels in obesity. This suggests that the differences in adipose glutamine release are dependent on the contribution from several resident cell types. Transcriptomic analyses demonstrated a strong negative association between *GLUL* and genes involved in pro-inflammatory processes, a link that was corroborated at the protein level by the negative correlations between *GLUL* and pro-inflammatory adipokine secretion from WAT.

Anti-inflammatory effects of GLUL-mediated glutamine production have been described in several cell types including murine microglia (Palmieri et al., 2017a), T cells (Johnson et al., 2018; Klysz et al., 2015; Metzler et al., 2016), and macrophages (Palmieri et al., 2017b; Ren et al., 2019), as well as adipocytes differentiated from a murine cell line (Palmieri et al., 2014). However, to our knowledge, the effects of glutamine on murine or human WAT inflammation have not been studied. To explore the effects of glutamine on WAT inflammation *in vivo*, we administered glutamine intraperitoneally in CD-fed mice. We chose this approach in order to avoid the confounding effects of glutamine-induced weight loss as previously reported (Abboud et al., 2019; Opara et al., 1996) as well as the effects on incretin release (Meek et al., 2015) and gut microbiota composition (de Souza et al., 2015) induced by oral administration. In this short-term intervention, the expression of a number of pro-inflammatory genes was attenuated without affecting any metabolic parameters, which encouraged us to extend the studies in an HFD

(K–P). Conditioned media in the *siOGT* experiments were collected for 48 h (days 9–11) while that in PUGNAc-treated cells was collected after 24 h (STAR Methods).

Statistical differences were analyzed by two-way ANOVA (glutamine and *siOGT*/PUGNAc, respectively) and results are shown for Tukey's post hoc test. ns, non-significant; Error bars are SEM. *$p < 0.05$, **$p < 0.01$, ***$p < 0.001$, ****$p < 0.0001$.

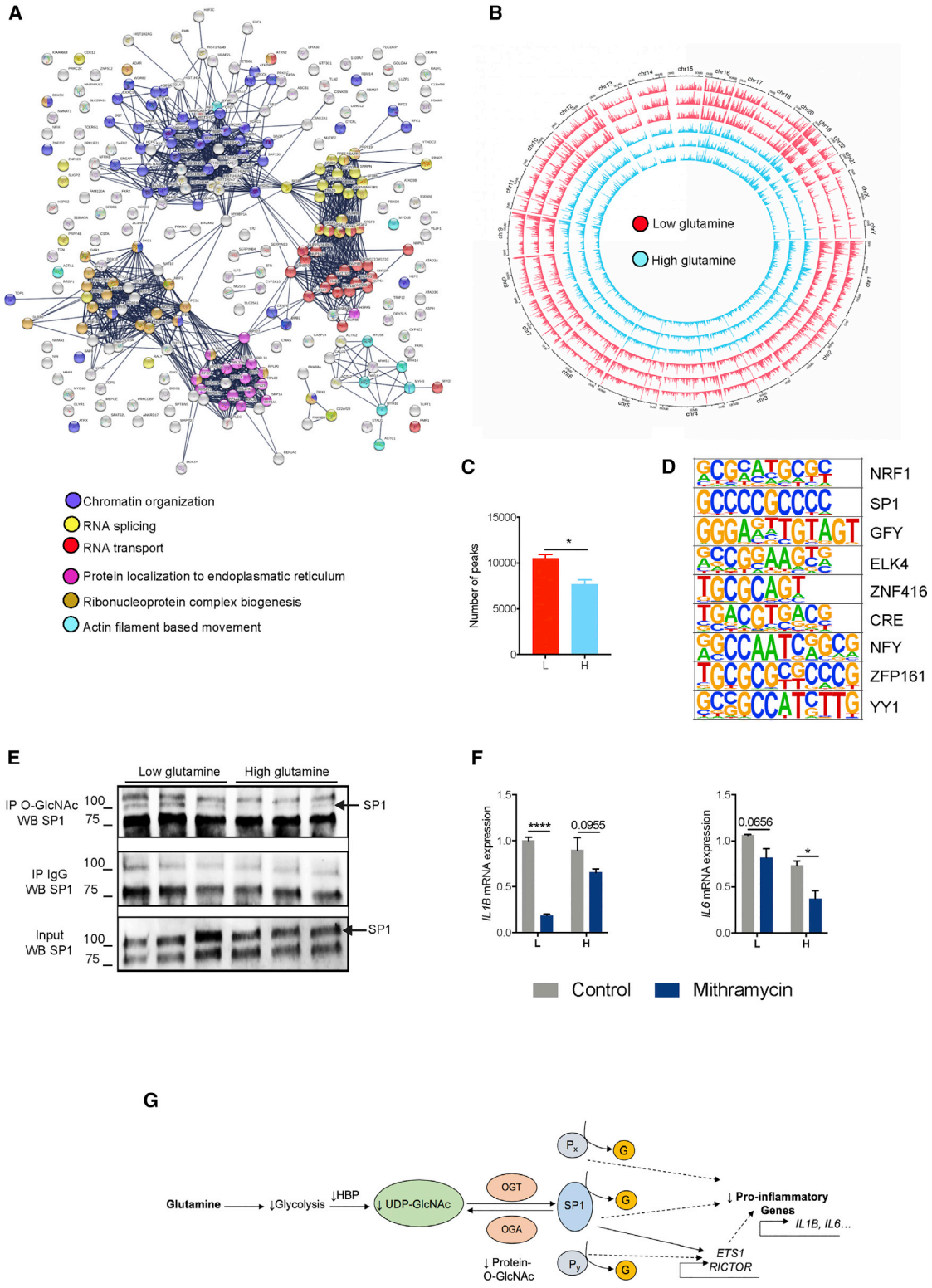

Figure 7. Mechanistic Insights into the Link between O-GlcNAcylation and Adipocyte Inflammation

(A) Nuclear lysates from human *in vitro* differentiated adipocytes were isolated and immunoprecipitated using an antibody directed against O-GlcNAc modified proteins. This was followed by proteomics analysis, which is represented according to their interactome. The common function of the proteins within interacting clusters is represented by colors as indicated.

(B) ChIP-seq analyses mapping the localization of the O-GlcNAcylation along the chromatin.

(legend continued on next page)

model. This intervention did not impact energy expenditure or respiratory exchange ratios and resulted only in small effects on WAT depot size and fat cell volume, but confirmed that glutamine normalized pro-inflammatory gene expression, F4/80 staining, and the proportion of M1 macrophages in WAT. Reductions in fasting plasma glucose and insulin were also observed in these animals, but no effects on glucose tolerance. Although this may indicate modest effects of glutamine on overall glucose metabolism, it could also be due to the relatively short intervention (2 weeks), which was determined by our animal handling regulations. Combined, this suggests that glutamine has direct effects on WAT inflammation, which may contribute to the beneficial metabolic effects of long-term glutamine supplementation. In *in vitro* differentiated human adipocytes, we could confirm a concentration- and time-dependent effect of glutamine on pro-inflammatory gene expression. While this was independent of effects on differentiation, reduced lipid droplet size was observed in cells incubated with high glutamine. This observation is congruent with the clinical correlations as well as the effects on murine fat cell size *in vivo* and suggests that glutamine induces metabolic changes that attenuate lipid accumulation and adipocyte hypertrophy.

Several mechanisms have been suggested to link glutamine and inflammation. In the Caco-2/TC7 enterocyte cell lines, it has been partly attributed to nuclear NF-κB degradation (Lesueur et al., 2012). In macrophages and T cells, it has been reported to be mediated via shifts in energy utilization (i.e., the balance between glycolysis and glutaminolysis), which alters the levels of intermediary metabolites such as α-ketoglutarate (Johnson et al., 2018; Klysz et al., 2015; Liu et al., 2017) or UDP-GlcNAc (Araujo et al., 2017; Swamy et al., 2016). Both these metabolites have been shown to regulate cell phenotype by acting as a co-substrate (α-ketoglutarate) or substrate (UDP-GlcNAc) for enzymes controlling either DNA/histone de-methylation (Johnson et al., 2018; Liu et al., 2017) or protein O-GlcNAcylation (Araujo et al., 2017; Swamy et al., 2016), respectively. Herein we demonstrate that high glutamine levels attenuated glycolysis, resulting in reduction of UDP-GlcNAc levels and O-GlcNAcylation. In contrast, no differences were observed in α-ketoglutarate levels or histone methylation, and incubation of human adipocytes with α-ketoglutarate did not impact the expression of inflammatory genes (data not shown). A causal link between glutamine-regulated O-GlcNAcylation and pro-inflammatory adipokine secretion in human adipocytes was demonstrated by several different approaches including *OGT* knockdown and pharmacological inhibition of either OGT or OGA. Yet as discussed further below, our data indicate that glutamine might also regulate inflammation via other mechanisms.

To gain insights into the processes influenced by O-GlcNAcylation in human adipocytes, we performed a proteomics analysis of the nuclear O-GlcNAcylated proteins that identified hundreds of proteins involved in chromatin remodeling, RNA processing, and ribosome biogenesis and transport. The role of O-GlcNAcylation in chromatin remodeling is well established (Lewis and Hanover, 2014). This modification on histones and transcription factor/co-factors can both activate and inhibit transcriptional activity (Slawson and Hart, 2011). Furthermore, O-GlcNAcylation of ribonuclear proteins has been previously reported in non-adipose cell lines (Ohn et al., 2008), but warrants further investigation in adipocytes. As O-GlcNAcylation of the spliceosome has not been reported, our data could be used to generate new hypotheses to investigate the link between O-GlcNAcylation and cellular processes. However, to establish the net contribution of each O-GlcNAcylated protein cluster to the adipose phenotype was outside the scope of the present study. Nevertheless, the spatial distribution of the O-GlcNAcylated proteome along the chromatin allowed mapping of the target regions affected by the glutamine-mediated changes in O-GlcNAcylation. These data confirmed the link between O-GlcNAcylation and inflammation. A bioinformatics approach to find transcription factors linking O-GlcNAcylation to inflammation identified SP1, which has previously been implicated in WAT inflammation (Kulyté et al., 2014). Moreover, O-GlcNAcylation of SP1 has been reported to have profound effects on its function by affecting its stability, nuclear translocation, and transcriptional activity (Yang and Qian, 2017), which in murine 3T3-F442a adipocytes results in altered cytokine expression (Wollaston-Hayden et al., 2015). In human adipocytes, the glutamine-mediated reduction in *IL1B* and *IL6* expression did not involve differential O-GlcNAcylation and/or SP1 binding to the corresponding promoters but rather indirect regulation of other genes. Bioinformatic analyses identified several genes related to inflammation where validation assays confirmed a link between glutamine, O-GlcNAcylation, and SP1. However, it must be stressed that the reduced SP1 O-GlcNAcylation is only one example and that the wide range of O-GlcNAcylated proteins suggests that glutamine-regulated O-GlcNAcylation may affect pro-inflammatory gene expression by additional mechanisms.

Although WAT inflammation is closely linked to metabolic dysfunction (Hotamisligil, 2006), therapies targeting inflammatory processes have not been successful in treating insulin

(C) Comparisons of the number of detected peaks from the ChIP-seq analysis in (B) in *in vitro* differentiated adipocytes treated with low (L, 0.5 mM) or high (H, 10 mM) glutamine.

(D) Homer motif enrichment analysis of the differentially O-GlcNAcylated sites from the ChIP-seq in (B).

(E) Nuclear lysates of *in vitro* differentiated human adipocytes incubated with high or low glutamine were immunoprecipitated with anti-OGlcNAc antibody (IP O-GlcNAc) and anti-mouse-IgG (negative control) and then subjected to western blot using an anti-SP1 antibody; input for SP1 in the nucleus lysates prior to immunoprecipitation is shown.

(F) *IL1B* (left panel) and *IL6* (right panel) expression in *in vitro* differentiated adipocytes treated low (L) and high (H) glutamine levels and with or without the SP1 inhibitor Mithramycin A.

(G) An illustration summarizing the mechanisms linking glutamine to transcriptional regulation of inflammatory genes. In this model, glutamine reduces UDP-GlcNAc and thereby protein O-GlcNAcylation through reduced glycolysis and HBP fluxes. The reduction in O-GlcNAcylation (symbolized by G) in multiple proteins (P_x, P_y) including SP1 leads to attenuated transcriptional activity at pro-inflammatory genes. Arrows with solid lines have been validated herein; dashed lines indicate hypothetical mechanisms.

Student's t tests were performed for comparison between groups. Error bars are SEM. *$p < 0.05$.

resistance or type 2 diabetes (Gao and Ye, 2012; Reilly and Saltiel, 2017). While this may depend on several mechanisms, recent data have re-appreciated the role of inflammation in WAT. Thus, transient activation of inflammation is essential for WAT expansion, and inhibition of these pathways may in fact be detrimental (Wernstedt Asterholm et al., 2014). This suggests that the link between inflammation and metabolic disease is dynamic and context dependent. It also indicates that WAT senses the local metabolic state resulting in an inflammatory response that enables tissue remodeling. Given the strong correlation between local glutamine levels/*GLUL* expression and adipocyte volume, one could speculate that increased adipocyte volume transiently activates inflammation by reducing local glutamine levels in order to allow WAT expansion. This is reversed once energy homeostasis has been achieved, a response that does not occur in conditions of constant caloric over-supply such as in obesity.

Conclusions

We report that glutamine metabolism is disturbed in WAT of obese individuals and correlates with a pernicious WAT phenotype. The reduced glutamine levels shift the balance from glutaminolysis toward glycolysis, leading to nuclear O-GlcNAcylation, which activates inflammation. Future studies are needed to understand the dynamics of this immunometabolic crosstalk and its potential therapeutic impact.

Limitations of Study

At the moment, we cannot define the relative importance of reduced glutamine release specifically in adipocytes for the overall effects on WAT inflammation. This would require cell-targeted knockout and/or overexpression of *GLUL in vivo*, but we cannot exclude that this could perturb intracellular metabolism and/or lead to compensatory changes in glutamine production in other resident cells. Our mechanistic studies focused on white adipocytes, and it remains to be demonstrated whether glutamine-mediated changes in O-GlcNAcylation play a similar role in adipose-resident leukocytes. Also, the full panorama of O-GlcNAc-dependent gene regulation needs to be explored in more detail. Furthermore, glutamine exerts effects on inflammation via non-O-GlcNAc-dependent mechanisms as well. This is demonstrated by the fact that CCL2 expression/release was not influenced by O-GlcNAc perturbation (see, e.g., Figures 6E, 6F, 6K, and 6L) and the observation that *IL1B* expression and IL6 secretion were lower in *siOGT*-transfected cells incubated in high versus low glutamine (compare pink bars in Figures 6G and 6J). These effects could be mediated via additional epigenetic modifications impacted by altered glycolysis, e.g., histone lactylation (Zhang et al., 2019). To unravel other mechanisms involved in glutamine-regulated inflammation in adipocytes will therefore be the focus of future studies.

STAR★METHODS

Detailed methods are provided in the online version of this paper and include the following:

- KEY RESOURCES TABLE
- LEAD CONTACT AND MATERIALS AVAILABILITY
- EXPERIMENTAL MODEL AND SUBJECT DETAILS
  - Subjects
  - Animals
  - Cell Cultures
- METHOD DETAILS
  - Clinical Examination
  - Animal Experiments
  - Histological Analysis
  - Metabolic Evaluations in Mice
  - Cell Culture Experiments
  - Cellular Lipid Staining
  - RNA Isolation, cDNA Synthesis and Real-Time PCR
  - Cell Sorting and RNA Expression Analysis of Human WAT Cell Populations
  - Isolation of Murine Stromal Vascular Fraction
  - Flow Cytometry of Murine Stromal Vascular Fraction
  - Transcriptomic Array
  - Chromatin Immunoprecipitation Sequencing
  - Cytokine Secretion
  - Immunoprecipitation of O-GlcNAcylated Proteins
  - Western Blot Analysis
  - Glucose Uptake Assay and Seahorse Extracellular Flux Analysis
  - Secreted Metabolomics Analysis
  - Cellular Untargeted Metabolomics Analysis
  - Proteomics Profiling
- QUANTIFICATION AND STATISTICAL ANALYSES
- DATA AND CODE AVAILABILITY

SUPPLEMENTAL INFORMATION

Supplemental Information can be found online at https://doi.org/10.1016/j.cmet.2019.11.019.

ACKNOWLEDGMENTS

We thank Elisabeth Dungner, Ana-Maria Suzuki, Katarina Hertel, Yvonne Widlund, Kerstin Wåhlén, Thais De Castro Barbosa, and Gaby Åström for excellent technical assistance. We would like also to acknowledge the bioinformatics and expression analysis (BEA) core facility in NEO at the Karolinska Institute for RNA sequencing and micro-array analyses, the proteomics core facility in Biomedicum at the Karolinska Institute for proteomics analyses, and Metabolon for metabolomics analyses. This work was supported by grants from the Swedish Research Council, the NovoNordisk Foundation (including the Tripartite Immuno-metabolism Consortium Grant Number NNF15CC0018486 and the MSAM consortium NNF15SA0018346), CIMED, the European Association on the Study of Diabetes together with Eli-Lilly, the Swedish Diabetes Foundation, the Knut and Alice Wallenberg Foundation (grant no. 2018.0094), the Stockholm County Council, the Diabetes Wellness Fund, and the Strategic Research Program in Diabetes at Karolinska Institutet.

AUTHOR CONTRIBUTIONS

P.P., S.L., and M.R. conceived the study, planned the experiments, collected all data, and wrote the first version of the manuscript. The final version was read and approved by all authors. L.D. and A.K. performed the glutamine study in mice. A.S. and M.A. performed the FACS analyses in murine WAT. C.W. and M.O.B. performed the bioenergetic study. H.G. contributed to the ChIP-seq analysis. B.T. and J.L. performed cytokine analyses, and J.L. and I.D. performed the cell sorting in human WAT. O.R. analyzed glutamine levels in human plasma samples. M.M., L.E., and R.P.C. contributed to data collection and performed part of the cellular analyses. P.A. contributed to the clinical phenotyping. A.C. and C.E.W. performed the metabolomics analyses of cohort 1. M.R. is the guarantor of this work.

DECLARATION OF INTERESTS

Following the initial submission of this work, M.M. has since June 2019 taken up a position as Senior Director and Staff Scientist at Genentech, Inc. and is a holder of Roche stock. However, neither he nor any other author of this work has any conflict of interest to report.

Received: February 18, 2019
Revised: August 27, 2019
Accepted: November 26, 2019
Published: December 19, 2019

REFERENCES

Abboud, K.Y., Reis, S.K., Martelli, M.E., Zordão, O.P., Tannihão, F., de Souza, A.Z.Z., Assalin, H.B., Guadagnini, D., Rocha, G.Z., Saad, M.J.A., and Prada, P.O. (2019). Oral glutamine supplementation reduces obesity, pro-inflammatory markers, and improves insulin sensitivity in DIO wistar rats and reduces waist circumference in overweight and obese humans. Nutrients *11*, 536.

Acosta, J.R., Joost, S., Karlsson, K., Ehrlund, A., Li, X., Aouadi, M., Kasper, M., Arner, P., Rydén, M., and Laurencikiene, J. (2017). Single cell transcriptomics suggest that human adipocyte progenitor cells constitute a homogeneous cell population. Stem Cell Res. Ther. *8*, 250.

Araujo, L., Khim, P., Mkhikian, H., Mortales, C.-L., and Demetriou, M. (2017). Glycolysis and glutaminolysis cooperatively control T cell function by limiting metabolite supply to N-glycosylation. eLife *6*, e21330.

Arner, E., Mejhert, N., Kulyté, A., Balwierz, P.J., Pachkov, M., Cormont, M., Lorente-Cebrián, S., Ehrlund, A., Laurencikiene, J., Hedén, P., et al. (2012). Adipose tissue microRNAs as regulators of CCL2 production in human obesity. Diabetes *61*, 1986–1993.

Arner, P., Andersson, D.P., Thörne, A., Wirén, M., Hoffstedt, J., Näslund, E., Thorell, A., and Rydén, M. (2013). Variations in the size of the major omentum are primarily determined by fat cell number. J. Clin. Endocrinol. Metab. *98*, E897–E901.

Berg, A., Rooyackers, O., Norberg, A., and Wernerman, J. (2005). Elimination kinetics of L-alanyl-L-glutamine in ICU patients. Amino Acids *29*, 221–228.

Berger, S.L., and Sassone-Corsi, P. (2016). Metabolic signaling to chromatin. Cold Spring Harb. Perspect. Biol. *8*, a019463.

Berry, R., Church, C.D., Gericke, M.T., Jeffery, E., Colman, L., and Rodeheffer, M.S. (2014). Imaging of adipose tissue. Methods Enzymol. *537*, 47–73.

Bhutia, Y.D., and Ganapathy, V. (2016). Glutamine transporters in mammalian cells and their functions in physiology and cancer. Biochim. Biophys. Acta *1863*, 2531–2539.

Cheng, S., Rhee, E.P., Larson, M.G., Lewis, G.D., McCabe, E.L., Shen, D., Palma, M.J., Roberts, L.D., Dejam, A., Souza, A.L., et al. (2012). Metabolite profiling identifies pathways associated with metabolic risk in humans. Circulation *125*, 2222–2231.

Cirulli, E.T., Guo, L., Leon Swisher, C., Shah, N., Huang, L., Napier, L.A., Kirkness, E.F., Spector, T.D., Caskey, C.T., Thorens, B., et al. (2019). Profound perturbation of the metabolome in obesity is associated with health risk. Cell Metab. *29*, 488–500.e2.

Crewe, C., An, Y.A., and Scherer, P.E. (2017). The ominous triad of adipose tissue dysfunction: inflammation, fibrosis, and impaired angiogenesis. J. Clin. Invest. *127*, 74–82.

Cruzat, V., Macedo Rogero, M., Noel Keane, K., Curi, R., and Newsholme, P. (2018). Glutamine: metabolism and immune function, supplementation and clinical translation. Nutrients *10*, E1564.

Dahlman, I., Kaaman, M., Olsson, T., Tan, G.D., Bickerton, A.S.T., Wåhlén, K., Andersson, J., Nordström, E.A., Blomqvist, L., Sjögren, A., et al. (2005). A unique role of monocyte chemoattractant protein 1 among chemokines in adipose tissue of obese subjects. J. Clin. Endocrinol. Metab. *90*, 5834–5840.

Dahlman, I., Sinha, I., Gao, H., Brodin, D., Thorell, A., Rydén, M., Andersson, D.P., Henriksson, J., Perfilyev, A., Ling, C., et al. (2015). The fat cell epigenetic signature in post-obese women is characterized by global hypomethylation and differential DNA methylation of adipogenesis genes. Int. J. Obes. *39*, 910–919.

Daskalaki, E., Pillon, N.J., Krook, A., Wheelock, C.E., and Checa, A. (2018). The influence of culture media upon observed cell secretome metabolite profiles: The balance between cell viability and data interpretability. Anal. Chim. Acta *1037*, 338–350.

de Souza, A.Z.Z., Zambom, A.Z., Abboud, K.Y., Reis, S.K., Tannihão, F., Guadagnini, D., Saad, M.J.A., and Prada, P.O. (2015). Oral supplementation with L-glutamine alters gut microbiota of obese and overweight adults: A pilot study. Nutrition *31*, 884–889.

Dehaven, C.D., Evans, A.M., Dai, H., and Lawton, K.A. (2010). Organization of GC/MS and LC/MS metabolomics data into chemical libraries. J. Cheminform. *2*, 9.

Donath, M.Y., and Shoelson, S.E. (2011). Type 2 diabetes as an inflammatory disease. Nat. Rev. Immunol. *11*, 98–107.

Etchegaray, J.P., and Mostoslavsky, R. (2016). Interplay between metabolism and epigenetics: a nuclear adaptation to environmental changes. Mol. Cell *62*, 695–711.

Evans, A.M., DeHaven, C.D., Barrett, T., Mitchell, M., and Milgram, E. (2009). Integrated, nontargeted ultrahigh performance liquid chromatography/electrospray ionization tandem mass spectrometry platform for the identification and relative quantification of the small-molecule complement of biological systems. Anal. Chem. *81*, 6656–6667.

Evans, A.M., Bridgewater, B., Liu, Q., Mitchell, M., Robinson, R., Dai, H., Stewart, S., DeHaven, C., and Miller, L. (2014). High resolution mass spectrometry improves data quantity and quality as compared to unit mass resolution mass spectrometry in high-throughput profiling metabolomics. Metabolomicsc *4*, https://doi.org/10.4172/2153-0769.1000132.

Frayn, K.N., Khan, K., Coppack, S.W., and Elia, M. (1991). Amino acid metabolism in human subcutaneous adipose tissue in vivo. Clin. Sci. (Lond.) *80*, 471–474.

Gabrielsson, B.G., Olofsson, L.E., Sjögren, A., Jernås, M., Elander, A., Lönn, M., Rudemo, M., and Carlsson, L.M.S. (2005). Evaluation of reference genes for studies of gene expression in human adipose tissue. Obes. Res. *13*, 649–652.

Gao, Z.G., and Ye, J.P. (2012). Why do anti-inflammatory therapies fail to improve insulin sensitivity? Acta Pharmacol. Sin. *33*, 182–188.

Gao, H., Mejhert, N., Fretz, J.A., Arner, E., Lorente-Cebrián, S., Ehrlund, A., Dahlman-Wright, K., Gong, X., Strömblad, S., Douagi, I., et al. (2014). Early B cell factor 1 regulates adipocyte morphology and lipolysis in white adipose tissue. Cell Metab. *19*, 981–992.

Gao, H., Volat, F., Sandhow, L., Galitzky, J., Nguyen, T., Esteve, D., Åström, G., Mejhert, N., Ledoux, S., Thalamas, C., et al. (2017). CD36 is a marker of human adipocyte progenitors with pronounced adipogenic and triglyceride accumulation potential. Stem Cells *35*, 1799–1814.

Goldrick, R.B., and McLoughlin, G.M. (1970). Lipolysis and lipogenesis from glucose in human fat cells of different sizes. Effects of insulin, epinephrine, and theophylline. J. Clin. Invest. *49*, 1213–1223.

Hill, J.O., Wyatt, H.R., Reed, G.W., and Peters, J.C. (2003). Obesity and the environment: where do we go from here? Science *299*, 853–855.

Hotamisligil, G.S. (2006). Inflammation and metabolic disorders. Nature *444*, 860–867.

Johnson, M.O., Wolf, M.M., Madden, M.Z., Andrejeva, G., Sugiura, A., Contreras, D.C., Maseda, D., Liberti, M.V., Paz, K., Kishton, R.J., et al. (2018). Distinct regulation of Th17 and Th1 cell differentiation by glutaminase-dependent metabolism. Cell *175*, 1780–1795.e19.

Kammoun, H.L., Kraakman, M.J., and Febbraio, M.A. (2014). Adipose tissue inflammation in glucose metabolism. Rev. Endocr. Metab. Disord. *15*, 31–44.

Kinouchi, K., Magnan, C., Ceglia, N., Liu, Y., Cervantes, M., Pastore, N., Huynh, T., Ballabio, A., Baldi, P., Masri, S., and Sassone-Corsi, P. (2018). Fasting imparts a switch to alternative daily pathways in liver and muscle. Cell Rep. *25*, 3299–3314.e6.

Kirwan, J.A., Broadhurst, D.I., Davidson, R.L., and Viant, M.R. (2013). Characterising and correcting batch variation in an automated direct infusion

mass spectrometry (DIMS) metabolomics workflow. Anal. Bioanal. Chem. *405*, 5147–5157.

Klysz, D., Tai, X., Robert, P.A., Craveiro, M., Cretenet, G., Oburoglu, L., Mongellaz, C., Floess, S., Fritz, V., Matias, M.I., et al. (2015). Glutamine-dependent α-ketoglutarate production regulates the balance between T helper 1 cell and regulatory T cell generation. Sci. Signal. *8*, ra97.

Kraakman, M.J., Kammoun, H.L., Allen, T.L., Deswaerte, V., Henstridge, D.C., Estevez, E., Matthews, V.B., Neill, B., White, D.A., Murphy, A.J., et al. (2015). Blocking IL-6 trans-signaling prevents high-fat diet-induced adipose tissue macrophage recruitment but does not improve insulin resistance. Cell Metab. *21*, 403–416.

Kučera, J., Spáčil, Z., Friedecký, D., Novák, J., Pekař, M., and Bienertová-Vašků, J. (2018). Human white adipose tissue metabolome: current perspective. Obesity (Silver Spring) *26*, 1870–1878.

Kulyté, A., Belarbi, Y., Lorente-Cebrián, S., Bambace, C., Arner, E., Daub, C.O., Hedén, P., Rydén, M., Mejhert, N., and Arner, P. (2014). Additive effects of microRNAs and transcription factors on CCL2 production in human white adipose tissue. Diabetes *63*, 1248–1258.

Laviano, A., Molfino, A., Lacaria, M.T., Canelli, A., De Leo, S., Preziosa, I., and Rossi Fanelli, F. (2014). Glutamine supplementation favors weight loss in non-dieting obese female patients. A pilot study. Eur. J. Clin. Nutr. *68*, 1264–1266.

Lee, Y.S., Wollam, J., and Olefsky, J.M. (2018). An integrated view of immunometabolism. Cell *172*, 22–40.

Lesueur, C., Bôle-Feysot, C., Bekri, S., Husson, A., Lavoinne, A., and Brasse-Lagnel, C. (2012). Glutamine induces nuclear degradation of the NF-κB p65 subunit in Caco-2/TC7 cells. Biochimie *94*, 806–815.

Lewis, B.A., and Hanover, J.A. (2014). O-GlcNAc and the epigenetic regulation of gene expression. J. Biol. Chem. *289*, 34440–34448.

Li, H., and Durbin, R. (2009). Fast and accurate short read alignment with Burrows-Wheeler transform. Bioinformatics *25*, 1754–1760.

Liu, P.-S., Wang, H., Li, X., Chao, T., Teav, T., Christen, S., Di Conza, G., Cheng, W.-C., Chou, C.-H., Vavakova, M., et al. (2017). α-ketoglutarate orchestrates macrophage activation through metabolic and epigenetic reprogramming. Nat. Immunol. *18*, 985–994.

Mansour, A., Mohajeri-Tehrani, M.R., Qorbani, M., Heshmat, R., Larijani, B., and Hosseini, S. (2015). Effect of glutamine supplementation on cardiovascular risk factors in patients with type 2 diabetes. Nutrition *31*, 119–126.

Mathis, D., and Shoelson, S.E. (2011). Immunometabolism: an emerging frontier. Nat. Rev. Immunol. *11*, 81–83.

Meek, C.L., Reimann, F., Park, A.J., and Gribble, F.M. (2015). Can encapsulated glutamine increase GLP-1 secretion, improve glucose tolerance, and reduce meal size in healthy volunteers? A randomised, placebo-controlled, cross-over trial. Lancet *385* (*Suppl 1*), S68.

Metzler, B., Gfeller, P., and Guinet, E. (2016). Restricting glutamine or glutamine-dependent purine and pyrimidine syntheses promotes human T cells with high FOXP3 expression and regulatory properties. J. Immunol. *196*, 3618–3630.

Morgantini, C., Jager, J., Li, X., Levi, L., Azzimato, V., Sulen, A., Barreby, E., Xu, C., Tencerova, M., Näslund, E., et al. (2019). Liver macrophages regulate systemic metabolism through non-inflammatory factors. Nat. Metab. *1*, 445–459.

Nagao, H., Nishizawa, H., Tanaka, Y., Fukata, T., Mizushima, T., Furuno, M., Bamba, T., Tsushima, Y., Fujishima, Y., Kita, S., et al. (2018). Hypoxanthine secretion from human adipose tissue and its increase in hypoxia. Obesity (Silver Spring) *26*, 1168–1178.

Naz, S., Gallart-Ayala, H., Reinke, S.N., Mathon, C., Blankley, R., Chaleckis, R., and Wheelock, C.E. (2017). Development of a liquid chromatography-high resolution mass spectrometry metabolomics method with high specificity for metabolite identification using all ion fragmentation acquisition. Anal. Chem. *89*, 7933–7942.

Ohn, T., Kedersha, N., Hickman, T., Tisdale, S., and Anderson, P. (2008). A functional RNAi screen links O-GlcNAc modification of ribosomal proteins to stress granule and processing body assembly. Nat. Cell Biol. *10*, 1224–1231.

Opara, E.C., Petro, A., Tevrizian, A., Feinglos, M.N., and Surwit, R.S. (1996). L-glutamine supplementation of a high fat diet reduces body weight and attenuates hyperglycemia and hyperinsulinemia in C57BL/6J mice. J. Nutr. *126*, 273–279.

Palmieri, E.M., Spera, I., Menga, A., Infantino, V., Iacobazzi, V., and Castegna, A. (2014). Glutamine synthetase desensitizes differentiated adipocytes to proinflammatory stimuli by raising intracellular glutamine levels. FEBS Lett. *588*, 4807–4814.

Palmieri, E.M., Menga, A., Lebrun, A., Hooper, D.C., Butterfield, D.A., Mazzone, M., and Castegna, A. (2017a). Blockade of glutamine synthetase enhances inflammatory response in microglial cells. Antioxid. Redox Signal. *26*, 351–363.

Palmieri, E.M., Menga, A., Martín-Pérez, R., Quinto, A., Riera-Domingo, C., De Tullio, G., Hooper, D.C., Lamers, W.H., Ghesquière, B., McVicar, D.W., et al. (2017b). Pharmacologic or genetic targeting of glutamine synthetase skews macrophages toward an M1-like phenotype and inhibits tumor metastasis. Cell Rep. *20*, 1654–1666.

Petrus, P., Bialesova, L., Checa, A., Kerr, A., Naz, S., Bäckdahl, J., Gracia, A., Toft, S., Dahlman-Wright, K., Hedén, P., et al. (2018a). Adipocyte expression of SLC19A1 links DNA hypermethylation to adipose tissue inflammation and insulin resistance. J. Clin. Endocrinol. Metab. *103*, 710–721.

Petrus, P., Mejhert, N., Corrales, P., Lecoutre, S., Li, Q., Maldonado, E., Kulyté, A., Lopez, Y., Campbell, M., Acosta, J.R., et al. (2018b). Transforming growth factor-β3 regulates adipocyte number in subcutaneous white adipose tissue. Cell Rep. *25*, 551–560.e5.

Pettersson, A.M.L., Stenson, B.M., Lorente-Cebrián, S., Andersson, D.P., Mejhert, N., Krätzel, J., Aström, G., Dahlman, I., Chibalin, A.V., Arner, P., and Laurencikiene, J. (2013). LXR is a negative regulator of glucose uptake in human adipocytes. Diabetologia *56*, 2044–2054.

Reid, M.A., Dai, Z., and Locasale, J.W. (2017). The impact of cellular metabolism on chromatin dynamics and epigenetics. Nat. Cell Biol. *19*, 1298–1306.

Reilly, S.M., and Saltiel, A.R. (2017). Adapting to obesity with adipose tissue inflammation. Nat. Rev. Endocrinol. *13*, 633–643.

Ren, W., Xia, Y., Chen, S., Wu, G., Bazer, F.W., Zhou, B., Tan, B., Zhu, G., Deng, J., and Yin, Y. (2019). Glutamine metabolism in macrophages: a novel target for obesity/type 2 diabetes. Adv. Nutr. *10*, 321–330.

Rosen, E.D., and Spiegelman, B.M. (2014). What we talk about when we talk about fat. Cell *156*, 20–44.

Slawson, C., and Hart, G.W. (2011). O-GlcNAc signalling: implications for cancer cell biology. Nat. Rev. Cancer *11*, 678–684.

Swamy, M., Pathak, S., Grzes, K.M., Damerow, S., Sinclair, L.V., van Aalten, D.M.F., and Cantrell, D.A. (2016). Glucose and glutamine fuel protein O-GlcNAcylation to control T cell self-renewal and malignancy. Nat. Immunol. *17*, 712–720.

Tchoukalova, Y.D., Harteneck, D.A., Karwoski, R.A., Tarara, J., and Jensen, M.D. (2003). A quick, reliable, and automated method for fat cell sizing. J. Lipid Res. *44*, 1795–1801.

Weisberg, S.P., McCann, D., Desai, M., Rosenbaum, M., Leibel, R.L., and Ferrante, A.W., Jr. (2003). Obesity is associated with macrophage accumulation in adipose tissue. J. Clin. Invest. *112*, 1796–1808.

Wernstedt Asterholm, I., Tao, C., Morley, T.S., Wang, Q.A., Delgado-Lopez, F., Wang, Z.V., and Scherer, P.E. (2014). Adipocyte inflammation is essential for healthy adipose tissue expansion and remodeling. Cell Metab. *20*, 103–118.

Wollaston-Hayden, E.E., Harris, R.B.S., Liu, B., Bridger, R., Xu, Y., and Wells, L. (2015). Global O-GlcNAc levels modulate transcription of the adipocyte secretome during chronic insulin resistance. Front. Endocrinol. (Lausanne) *5*, 223.

Yang, X., and Qian, K. (2017). Protein O-GlcNAcylation: emerging mechanisms and functions. Nat. Rev. Mol. Cell Biol. *18*, 452–465.

Yelamanchi, S.D., Jayaram, S., Thomas, J.K., Gundimeda, S., Khan, A.A., Singhal, A., Keshava Prasad, T.S., Pandey, A., Somani, B.L., and Gowda, H. (2016). A pathway map of glutamate metabolism. J. Cell Commun. Signal. *10*, 69–75.

Zhang, D., Tang, Z., Huang, H., Zhou, G., Cui, C., Weng, Y., Liu, W., Kim, S., Lee, S., Perez-Neut, M., et al. (2019). Metabolic regulation of gene expression by histone lactylation. Nature *574*, 575–580.

STAR★METHODS

KEY RESOURCES TABLE

REAGENT or RESOURCE	SOURCE	IDENTIFIER
Antibodies		
O-Linked N-Acetylglucosamine (RL2) (WB:1:1000; ChIP: 5 μg; IP: 5 μg)	Abcam	Cat#ab2739; RRID: AB_303264
SP1 (ChIP: 5 μg)	Abcam	Cat#ab13370; RRID: AB_300283
OGT/O-GlcNAc transferase (WB: 1:500)	Active Motif	Cat#61355; RRID: AB_2793604
SP1 (ChIP: 5 μg)	Active Motif	Cat#39058; RRID: AB_2793151
CD3 APC (Flow Cytometry, FC: 1:20)	BD Biosciences	Cat#340661; RRID: AB_400530
CD11c PE (FC: 1:200)	BD Biosciences	Cat#553802; RRID: AB_395061
CD14 BV711 (FC: 1:40)	BD Biosciences	Cat#563372; RRID: AB_2744290
CD11b PE-Cy7 (FC: 1:200)	BD Biosciences	Cat#561098; RRID: AB_2033994
CD31 FITC (FC: 1:5)	BD Biosciences	Cat#557508; RRID: AB_396739
CD34 PE-CF594 (FC: 1:125)	BD Biosciences	Cat#562449; RRID: AB_11152083
CD45 PE-CF594 (FC: 1:1000)	BD Biosciences	Cat#562420; RRID: AB_11154401
CD45 Alexa Fluor 700 (FC: 1:50)	BD Biosciences	Cat#560566; RRID: AB_1645452
Siglec-F BB515 (FC: 1:200)	BD Biosciences	Cat#564514; RRID: AB_2738833
CD19 PE-Cy5 (FC: 1/200)	Biolegend	Cat#115510; RRID: AB_313645
F4/80 Alexa Fluor 647 (Immunohistofluoresence: 1:200)	Biolegend	Cat#123121; RRID: AB_893492
F4/80 (FC: 1:50)	Bio-Rad	Cat#MCA497APC; RRID: AB_324435
Lamin A/C (WB: 1:2500)	Cell Signaling	Cat#4777; RRID: AB_10545756
α-Tubulin (WB: 1:1000)	Cell Signaling	Cat#2144; RRID: AB_2210548
SP1 (WB: 1:500)	Santa Cruz Biotechnology	Cat#Sc-420; RRID: AB_628271
Actin (WB: 1:1000)	Sigma-Aldrich	Cat#A2066; RRID: AB_476693
Anti-Rabbit IgG-HRP (WB: 1:10000)	Sigma-Aldrich	Cat#A9169; RRID: AB_258434
Anti-Mouse IgG-HRP (WB: 1:10000)	Sigma-Aldrich	Cat#5278; RRID: AB_258232
GLUL (WB: 1:1000)	Sigma-Aldrich	Cat#WH0002752M1; RRID: AB_1841781
Normal Mouse IgG (ChIP: 5 μg; IP: 5 μg)	Sigma-Aldrich	Cat#12-371
Biological Samples		
Human subcutaneous and visceral fat biopsies	This paper	N/A
Human *in vitro* differentiated adipocytes	This paper and previous work from the group	Gao et al., 2017
Chemicals, Peptides, and Recombinant Proteins		
TaqMan Master Mix	Applied Biosystems	Cat#4318157
7-aminoactinomycin D	BD Biosciences	Cat#559925
SYBR-green Master Mix	Bio-Rad	Cat#1708884
Mithramycin A	Cayman	Cat#11434
Amersham ECL Prime Blocking Reagent	GE Healthcare	Cat#RPN418
Amersham ECL Prime Western Blotting Detection Reagent	GE Healthcare	Cat#RPN2232
Glutamine Solution	GE Healthcare	Cat#SH30034.01
DMEM	Lonza	Cat#12-708F
2-deoxy-D-glucose	PerkinElmer	Cat#NET328250UC
QIAzol lysis reagent	QIAGEN	Cat#79306
HiPerFect	QIAGEN	Cat#301707
LipidTox	ThermoFisher	Cat#H34476
Hoechst	ThermoFisher	Cat#H3570
CellMask	ThermoFisher	Cat#C10045

(*Continued on next page*)

Continued

REAGENT or RESOURCE	SOURCE	IDENTIFIER
Glucose Solution	ThermoFisher	Cat#A2494001
DMEM	ThermoFisher	Cat#21700-026
Ham's F-12 Nutrient Mix	ThermoFisher	Cat#11765054
RIPA buffer	ThermoFisher	Cat#89901
Dynabeads protein G	ThermoFisher	Cat#1004D
SYTOX Blue	ThermoFisher	Cat#S34857
CountBright Absolute Counting Beads	ThermoFisher	Cat#C36950
Pierce Protein A/G magnetic beads	ThermoFisher	Cat#88802
RIPA buffer	ThermoFisher	Cat#89901
Collagenase	Sigma-Aldrich	Cat#C6885
2-deoxy-D-glucose	Sigma-Aldrich	Cat#D6134-1G
PUGNAc	Sigma-Aldrich	Cat#A7229
GalNAc-O-bn	Sigma-Aldrich	Cat#B4894
FGF2, Fibroblast Growth Factor-Basic human, bFGF	Sigma-Aldrich	Cat#F0291-4X25UG
HyClone FBS, EU approved South American Origin	Hyclone, GE	Cat#SV30160-03
Critical Commercial Assays		
Seahorse XF Glycolysis Stress Test	Agilent	Cat#103020-100
Seahorse XFp Mito Fuel Flex Test	Agilent	Cat#103070-100
iSript cDNA Synthesis kit	Bio-Rad	Cat#170-8891
Insulin ELISA Kit	Crystal Chem	Cat#90080
EZ-Magna ChIP HiSens Chromatin Immunoprecipitation Kit	Merck	Cat#17-10461
V-plex Plus Human IL-1b kit	Mesoscale Discovery	Cat#K151QP
NEBnext chip-seq library Prep master mix set	New England Biolabs	Cat#E6240L
EZBlue Gel Staining Reagent	Sigma-Aldrich	Cat#G1041
Pierce BCA Protein Assay Kit	ThermoFisher	Cat#23227
20-plex Human panel	ThermoFisher	EXP200-12185-901
MCP-1/CCL2 Human ELISA Kit	ThermoFisher	Cat#88-7399-22
IL-6 Human ELISA Kit	ThermoFisher	Cat#KHC0061
RNeasy Lipid Tissue Mini Kit	QIAGEN	Cat#74804
NucleoSpin RNA	Macherey-Nagel	Cat#740955.250
Deposited Data		
Human gene expression data (gene microarray)	This paper	GEO: GSE59034
Human *in vitro* differentiated adipocytes incubated in high and low glutamine (gene microarray)	This paper	GEO: GSE140426
SP1 RNAi in human *in vitro* differentiated adipocytes (gene microarray)	This paper	GEO: GSE140426
O-GlcNAc ChIPseq (sequencing data)	This paper	GEO: GSE140426
Experimental Models: Organisms/Strains		
Mouse C57/BL/6J	Charles River	N/A
Oligonucleotides		
TaqMan probe human *LRP10*	Applied Biosystems	Hs00204094_m1
TaqMan probe human *PPIA*	Applied Biosystems	Hs04194521_s1
TaqMan probe human *OGN*	Applied Biosystems	Hs00247901_m1
TaqMan probe human *CCL2*	Applied Biosystems	Hs00234140_m1
TaqMan probe human *IL1B*	Applied Biosystems	Hs01555410_m1
TaqMan probe human *IL6*	Applied Biosystems	Hs00985639_m1
TaqMan probe human *ADIPOQ*	Applied Biosystems	Hs00605917_m1
TaqMan probe human *PLIN1*	Applied Biosystems	Hs00193510_m1
TaqMan probe human *PNPLA2*	Applied Biosystems	Hs00386101_m1
TaqMan probe human *PPARG*	Applied Biosystems	Hs01115513_m1

(*Continued on next page*)

Continued

REAGENT or RESOURCE	SOURCE	IDENTIFIER
TaqMan probe human *GLUL*	Applied Biosystems	Hs00365928_g1
TaqMan probe human *CEBPA*	Applied Biosystems	Hs00269972_s1
TaqMan probe human *ENO1*	Applied Biosystems	Hs00361415_m1
TaqMan probe human *HK2*	Applied Biosystems	Hs00606086_m1
TaqMan probe human *PFKFB3*	Applied Biosystems	HS00998700_m1
TaqMan probe human *RICTOR*	Applied Biosystems	Hs00380903_m1
TaqMan probe human *ETS1*	Applied Biosystems	Hs00901425_m1
TaqMan probe murine *Adipoq*	Applied Biosystems	Mm00456425_m1
TaqMan probe murine *Ccl2*	Applied Biosystems	Mm00441242_m1
TaqMan probe murine *ActB*	Applied Biosystems	Mm00607939_s1
TaqMan probe murine *Il6*	Applied Biosystems	Mm00446190_m1
TaqMan probe murine *Gapdh*	Applied Biosystems	Mm99999915_g1
TaqMan probe murine *Tnf*	Applied Biosystems	Mm00443258_m1
TaqMan probe murine *Pparg*	Applied Biosystems	Mm00440940_m1
SYBR green probe murine *Emr1*; Fw:TGACTCACCTTGTGGTCCTAA; Rv:CTTCCCAGAATCCAGTCTTTCC	Sigma-Aldrich	N/A
SYBR green probe murine *Cd68*; Fw:TGTCTGATCTTGCTAGGACCG; Rv:GAGAGTAACGGCCTTTTTGTGA	Sigma-Aldrich	N/A
SYBR green probe murine *Glul*; Fw:TTAGGGGAATTAAGGACAGG; Rv:GAAGGAAAGTAACAGTCTGC	Sigma-Aldrich	N/A
SYBR green probe murine *Il1b*; Fw:CAACCACACTCTCCAGCTGCA; Rv:GATCCACACTCTCCAGCTGCA	Sigma-Aldrich	N/A
SYBR green probe murine *Col6a1*; Fw:CTGCTGCTACAAGCCTGCT; Rv:CCCCATAAGGTTTCAGCCTCA	Sigma-Aldrich	N/A
SYBR green probe human *ETS1 ChIP-qPCR*; Fw:CGCTCTCCCCTC CTCTTTAG; Rv:CAGCCCTTCCTTTCGCTTTG	Sigma-Aldrich	N/A
SYBR green probe human *RICTOR ChIP-qPCR*; Fw:GTCACAACACC GGAAACCTC; Rv:CGAACTCCTTGCAGACCTTG	Sigma-Aldrich	N/A
SYBR green probe human *PFKFB3 ChIP-qPCR*; Fw:AAGATGCCGTT GGAACTGAC; Rv:AAAGCCGCCCCACACAAT	Sigma-Aldrich	N/A
siRNA anti human *OGT* (siGENOME)	Dharmacon	M-019111-00-0005
siRNA anti human *HK2* (siGENOME)	Dharmacon	M-006735-01-0005
siRNA anti human *ENO1* (siGENOME)	Dharmacon	M-004034-02-0005
siRNA Non-targeting #1 (siGENOME)	Dharmacon	D-001206-13-05
siRNA anti human *SP1* (pool of 3 siRNA)	QIAGEN	siSP1.1#SI02648072, siSP1.2#SI02648065, siSP1.3#SI00150990
siRNA Non-targeting	QIAGEN	Cat#1027310
Software and Algorithms		
Image Lab	Bio-Rad	N/A
GraphPad Prism 7.0	GraphPad Software	N/A
SPSS v24	IBM	N/A
FlowJo	Tree Star	https://www.flowjo.com/
DAVID	NIAID/NIH	https://david.ncifcrf.gov
ImageJ 1.45 software	NIH	N/A
HOMER	N/A	http://homer.ucsd.edu
Other		
Standard chow diet (4% kcal from fat)	Lantmännen	R34
High Fat Diet (HFD; 60% kcal fat)	Research Diet	D12492i

LEAD CONTACT AND MATERIALS AVAILABILITY

Further information and requests for resources and reagents should be directed to and will be fulfilled by the Lead Contact Mikael Rydén (mikael.ryden@ki.se). This study did not generate unique reagents.

EXPERIMENTAL MODEL AND SUBJECT DETAILS

Subjects

Three cohorts were investigated (clinical characteristics in Table S1). Cohort 1 comprised 81 (29 non-obese mean ± S.D: age 44 ± 13 years, BMI 24 ± 3 kg/m^2 and 52 obese age 43 ± 10 years, BMI 38 ± 3 kg/m^2) women recruited in a study investigating the effects of bariatric surgery (NCT01727245). Only baseline data are reported herein. Abdominal subcutaneous white adipose tissue (WAT) biopsies were available in all, serum samples were available in 53 individuals. Samples in sub-cohort 1 were obtained from 13 non-obese and 13 obese individuals which were selected depending on availability of additional adipose tissue samples. Cohort 2 consisted of 26 non-obese (age 43 ± 14 years, BMI 24 ± 2 kg/m^2) and 30 obese (age 43 ± 10 years, BMI 41 ± 7 kg/m^2) women and has been described in detail previously (Arner et al., 2012). They were subdivided into WAT hypertrophy/hyperplasia as described (Gao et al., 2014). Cohort 3 consisted of 15 obese women before (age 47.7 ± 8.6 years, BMI 41 ± 5 kg/m^2) and two years after bariatric surgery (BMI 25 ± 3 kg/m^2). They were matched with 15 healthy never obese control women for age (49.3 ± 9.4 years) and BMI (25 ± 2 kg/m^2) at the two year follow up (Dahlman et al., 2015; Petrus et al., 2018a). The reason only women were included in the three cohorts is that the vast majority of obese subjects undergoing bariatric surgery in Sweden are females. For cohort 1, it is difficult to calculate sample size for untargeted secreted metabolomics as there are no prior data from human adipose tissue. A power calculation based on the reported human adipose tissue secretion of CCL2 (mean ± SD) from non-obese and obese women (Dahlman et al., 2005) showed that we had 80% power to detect a mean difference of 35% at alpha = 0.05 with 27 individuals in each group. Cohorts 2-3 have been published and no power calculation was performed the present study. However, they were numerically large and data in cohort 2 was confirmed at the protein level (Figures 2B–2D) and in cohort 3 by qPCR (Figure 1J). In subjects scheduled for bariatric surgery, WAT biopsies were performed in local anesthesia several weeks prior to surgery. The main reason is that these subjects are routinely asked to start with very low calorie diet two weeks prior to surgery; an intervention that has pronounced effects on WAT gene expression and function. All studies were approved by the regional board of ethics and informed written consent was obtained from each subject.

Animals

Chow Diet Study

C57BL/6J male mice were purchased from Charles River (Germany) and fed a standard rodent chow diet (4% kcal from fat, R34; Lantmännen, Kimstad, Sweden). Mice were group housed (4 per cage) in ventilated cages with a 12 h light/12 h dark cycle (lights on 06:00–18:00), temperature-controlled (20-24°C) facility, with *ad libitum* access to food and water. At 11 weeks of age, mice were randomized to treatment group (n = 8/group) based on body weight and received daily intraperitoneal injection of glutamine (1 g/kg body weight) or phosphate buffered saline (PBS) (20 mL/kg body weight) for 14 days. This time span was based on the regulations of the Animal Ethical Committee.

High Fat Diet Study

Mice were purchased and housed as described above, with *ad libitum* access to food and water. At 6-8 weeks of age, mice were fed either a standard chow diet (4% kcal from fat, R34; Lantmännen) or a 60% fat diet (Research Diet, New Brunswick, NJ) for 5 weeks. After 3 weeks into the high fat diet (HFD) intervention, mice were randomized to treatment group (n = 8-12/group) based on body weight and body composition and received daily intraperitoneal injection of glutamine (1 g/kg body weight) or PBS (20 mL/kg body weight) for 14 days. The timing of HFD and glutamine treatment in these experiments were based on separate qPCR analyses of *Glul* mRNA expression in eWAT samples obtained from a previous study (Morgantini et al., 2019) where mice were put on chow or HFD for 3, 9 and 12 weeks. This showed that *Glul* was significantly downregulated already after 3 weeks on HFD.

In both experiments, animals were handled following the European Union laws and guidelines for animal care. Mice were purchased pathogen-free and housed in the animal facility at Karolinska Institutet. Health inventories are performed on a regular basis (every 3 months) and follow the guidelines of the Federation of European Laboratory Animal Science Associations (FELASA) (http://www.felasa.eu/working-groups/working-groups-past/revision-of-guidelines-for-health-monitoring-of-rodent-and-rabbits). Experimental procedures were approved by the Stockholm North Animal Ethical Committee (ethical permit N38/15), and special care was taken to minimize animal suffering and to reduce the number of animals used.

Cell Cultures

Cultures of *in vitro* differentiated human adipocytes were set up and differentiated as described (Petrus et al., 2018b). In brief, cells were obtained from abdominal subcutaneous white adipose tissue (sWAT) of one male donor. The adipose tissue was incubated in type II collagenase (Sigma-Aldrich) followed by isolation of the stroma vascular fraction (SVF) which includes the adipocyte progenitors. The cells were washed and subsequently expanded for 6-8 passages in proliferation medium (DMEM, 10 mmol/l HEPES, 10% FBS, 50 μg/mL Penicillin-Streptomycin) supplemented with 2.5 ng/mL Fibroblast growth factor-2 (FGF2) (Sigma-Aldrich, St Louis, MO). These cells are cryopreservable, undergo several passages (between 10-20) and are devoid of contaminating cells such as

leukocytes or endothelial cells. Cells were plated at a cell density of 20 000 cells/cm^2 and incubated at 37°C with 5% CO_2. Adipogenesis was induced two days post confluence using DMEM/F12 or DMEM without glucose/FGF2 containing 0-20 mM of glutamine concentrations and 1-50 mM glucose (for the entire incubation period, see below) as well as the adipogenic cocktail; 5 mg/mL insulin, 0.25 mmol/l dexamethasone, 0.5 mmol/l 3-isobutyl-1-methylxanthine (IBMX) and 10 mmol/l rosiglitazone for two days after which the dexamethasone and IBMX were removed and the cells were allowed to undergo full adipogenic differentiation. Please note that glutamine is required for O-GlcNAcylation as it functions as a co-substrate for the rate-limiting enzyme GFPT1 in the hexosamine biosynthetic pathway (Figure S5B) and that 0 mM glutamine is not physiologically relevant *in vivo*. No glutamine in the medium can therefore not be considered to constitute an adequate control.

METHOD DETAILS

Clinical Examination

After an overnight fast, anthropometric measures (height, weight, waist and hip circumferences) were determined and venous blood samples were obtained for routine clinical chemistry analyses. Body composition was determined by bioimpedance (Tanita, Tokyo, Japan) or by dual-X-ray absorptiometry (GE Luna iDXA, GE Health Care, Madison, WI) (Arner et al., 2013). A sWAT biopsy was obtained from the para-umbilical region by needle aspiration under local anesthesia. Methods for determination of WAT cellularity have been described in detail previously (Arner et al., 2013). In brief, isolated adipocytes were prepared by collagenase incubation. The diameter of 100 adipocytes were determined and shown to be normally distributed. Using established formulae (Goldrick and McLoughlin, 1970), these values were used to calculate average size and weight of the adipocytes in the WAT biopsy. The precision of the measures is not improved by increasing the number of counted cells (Tchoukalova et al., 2003) and is comparable to estimating cell size in intact tissue by histology, as discussed previously (Arner et al., 2013).

Animal Experiments

Four h before the sacrifice, body weight was measured and the total lean and fat mass was assessed in conscious mice using the EchoMRI-100 system (Echo Medical Systems). Plasma glucose was measured after 4 h of fasting using a glucometer (One Touch Ultra 2 Glucose Meter; Lifescan). Animals were euthanized under general anesthesia by avertin injection and the wet weight of each dissected tissue was measured. WAT was obtained from epigonadal regions (eWAT). Samples were snap-frozen in liquid nitrogen immediately after weight was determined except for one part (~50 mg) which was fixed in 4% formalin (pH 7.0) and used for histological analyses and another part which was kept for isolation of SVF for flow cytometric analysis of adipose tissue macrophages (ATMs).

Histological Analysis

Adipose tissue samples were fixed in 4% paraformaldehyde for 24 h, embedded in paraffin, and then sectioned (5 μm) and stained with hematoxylin and eosin (H & E; Sigma-Aldrich). For each sample, representative photomicrographs were acquired blindly with regard to treatment/diet from the whole section using the CellInsight CX5 High Content Screening (HCS) Platform (4X magnification). Average adipocyte size (Feret's diameter) in each animal was assessed using the ImageJ 1.45 software (National Institutes of Health, Bethesda, MD) and the macro MRI's adipocyte tool. Immunohistofluorescence was performed as previously described (Berry et al., 2014). In brief, sections were rehydrated by successive baths in xylene, ethanol and PBS followed by saturation (blocking solution) with 1% casein (ThermoFisher Scientific) for 1 h. Anti-F4/80 and Orange CellMask (1:5000) were diluted in the blocking solution as detailed in the Key Resources Table and added to the slides for 1 h. Sections were then washed in PBS 3x10 min and scanned using the CellInsight CX5 High Content Screening (HCS) Platform (10X magnification).

Metabolic Evaluations in Mice

For the HFD study in mice, body compositions were determined on day 1 and 15 of the treatment. Total lean and fat mass were assessed in conscious mice using the EchoMRI-100 system (Echo Medical Systems). Glucose tolerance was determined on a subgroup of mice at D11 of the treatment. Glucose (1 g/kg body weight) was administered by intraperitoneal injection in mice fasted for 4 h. Blood was sampled through the tail vein to measure glucose (OneTouch Ultra 2 glucose meter; LifeScan) and insulin (Insulin ELISA Kit; Crystal Chem). HOMA-IR was calculated as [(fP-glucose mM x fP-insulin mIU/l)/22.5]. Food intake, oxygen consumption, respiratory exchange ratio (RER) and locomotor activity (data not shown) were measured in a subgroup of mice from D10 to D14 of the treatment using a Comprehensive Lab Animal Monitoring System (Columbus Instruments, Columbus, OH). In brief, male mice were housed individually with *ad libitum* access to 60% fat diet and water. They were acclimatized to the metabolic cages for 24 h prior to a 48 h period of automated recordings every 25 min. Oxygen consumption (VO2) was determined by an open-circuit Oxymax. Sample air from individual cages was passed through sensors to determine O2 and CO2 content. Oxygen consumption was calculated as the difference between the input oxygen flow and the output oxygen flow. The respiratory exchange ratio (RER) was calculated as the ratio between the CO2 production and the O2 consumption. Energy expenditure (EE) was calculated using the formula (3.815+1.232xRER)xVO2 following the manufacturer recommendation. Ambulatory locomotor activity was measured by consecutive beam breaks in adjacent beams under the 48 h period.

Cell Culture Experiments

The differentiation media were supplemented with different glutamine concentrations ranging between 0-20 mM and different glucose concentrations ranging between 1-50 mM. Conditions with 50 mM glucose induced significant cellular toxicity and were therefore not considered in this article (data not shown). In the indicated experiments, cells were incubated with high or low glutamine during the entire differentiation period; at day 11 post-adipogenic induction they were treated with 100 μM 2-deoxyglucose (2DG), 200 μM PUGNAc, 10 μM mithramycin A or 1 mM GalNAc-*O*-bn for 24 h. RNA interference (RNAi) treatments were performed as previously described (Petrus et al., 2018b). In brief, short interfering oligonucleotides (siRNA) targeting *OGT*, *HK2* and *ENO1* were used and compared to cells transfected with non-targeting control siRNA (both from Dharmacon, see Key Resources Table for details). Cells were transfected with HiPerFect (QIAGEN, Germany) at day 0 after which adipocyte differentiation was induced as described above under high (10 mM) or low (0.5 mM) glutamine concentrations. Knockdown efficiency was determined in RNA isolated from the cells at day 11. For OGT, knockdown efficiency was also determined by western blot.

Cellular Lipid Staining

Cells were fixed in 4% PFA for 15 min at room temperature and washed twice with PBS. Cells were stained with lipidTOX green (diluted 1:1000) and Hoechst (diluted 1:5000) for 15 min to stain accumulated lipids. Cells were then washed four times with PBS and images were acquired using the CellInsight CX5 High Content Screening (HCS) Platform (10X magnification).

RNA Isolation, cDNA Synthesis and Real-Time PCR

Total RNA was extracted from intact human or murine WAT, mature adipocytes, SVF as well as cell cultures using column-based commercial kits (listed in the Key Resources Table) according to the provided instructions. The concentration, purity and quality were measured using Nanodrop 2000 (Thermo Fisher Scientific, Lafayette, CO) and Agilent 2100 Bioanalyzer (Agilent Technologies, Palo Alto, CA). Total RNA was reverse transcribed with iScript cDNA synthesis kits (Bio-Rad, Hercules, CA). Assessments of mRNA levels were performed using TaqMan assays (Applied Biosystems, Foster City, CA) or SYBR-green (Biorad) and relative expression was calculated with the comparative Ct-method, i.e., $2^{\Delta Ct\text{-target gene}}/2^{\Delta Ct\text{-reference gene}}$. The following probes were used (detailed in the Key Resources Table): *ADIPOQ, CCL2, C/EBPA, ENO1, ETS1, GLUL, HK2, IL1B, IL6, OGT, PFKFB3, PLIN1, PPARG, PNPLA2, RICTOR* and normalized against *PPIA* and *LRP10*. Murine gene expression was assessed using primers/probes targeting *Adipoq, Ccl2, Emr1, Cd68*, *Glul, Tnfa, Il1b, Col6a1, Pparg* and normalized against *Actb and Gapdh*.

Cell Sorting and RNA Expression Analysis of Human WAT Cell Populations

The SVF and mature adipocytes were prepared from human sWAT obtained by liposuctions/other plastic surgery procedures after collagenase treatment as described above as well as elsewhere (Petrus et al., 2018a). After several washing steps and centrifugation, floating mature adipocyte (MA) were collected from the supernatant, and SVF from the lower, aqueous phase. Fluorescence activated cell sorting (FACS) of SVF was performed as described (Acosta et al., 2017). In brief, cryopreserved SVF cells isolated from WAT were thawed, washed with PBS supplemented with 0.5% BSA (Sigma-Aldrich; A4503) and 2 mmol/l EDTA buffer and passed through a 70 μm cell mesh (BD Biosciences, San Diego, CA). The cells were stained for 30 min at 4°C with fluorophore-conjugated antibodies (listed in the Key Resources Table) in 50 μL BD Horizon Brilliant Stain Buffer (BD Biosciences). After staining, cells were washed, filtered again and re-suspended in PBS supplemented with 0.1% BSA and 2 mmol/l EDTA buffer. Cell viability was determined using tryphan blue. Adipocyte progenitor cells (APC) were defined as CD45-/CD31-/CD34+, adipose tissue macrophages (ATM) as CD45+/CD14+/CD206+, M1 macrophages CD45+/CD14+/CD206+/CD11c+, M2 macrophages CD45+/CD14+/CD206+/CD11c-, total T cells as CD45+/CD3+, CD8 T cells as CD45+/CD3+/CD8+ and CD4 T cells as CD45+/CD3+/CD4+. For the *in vitro* experiments the cells were incubated in RPMI (T cells and macrophages) or DMEM (progenitors) with 0.5 or 10 mM glutamine for 48 h followed by RNA isolation and collection of media. Mature adipocytes were washed after the collagenase treatment, pipetted with a tip with a wide opening and cultured in DMEM medium (Pettersson et al., 2013) containing 0.5 or 10 mM glutamine for 48 h followed by RNA isolation and collection of media. RNA quality in samples from total SVF, mature adipocytes, progenitor cells, leukocytes and macrophages were assessed by Agilent Bioanalyzer 2100 (Agilent Technologies, Santa Clara, CA), accepting RIN > 6.6. Quantitative PCR was performed for *CCL2*, *IL1B* and *IL6* (Figures 3M–3O); in ATMs, T cells and APCs *PPIA* was used as reference gene while *LRP10* was used in samples of mature adipocytes given that *LRP10* has been suggested as a preferred reference gene in adipose samples (Gabrielsson et al., 2005). For gene microarray analyses of SVF cells detailed in Figure 1N, RNA was analyzed on Clariom D Human assay (Thermo Fisher Scientific, Lafayette, CO) in accordance with the manufacturer's instructions as previously described (Acosta et al., 2017).

Isolation of Murine Stromal Vascular Fraction

Adipose tissue was minced with a scalpel and transferred to Hank's balanced salt solution (HBSS) containing 2% BSA and 1.4 mg/mL type II collagenase (Sigma-Aldrich). The samples were incubated at 37°C for 20 min with agitation. An equal amount of Dulbecco's modified eagle medium (DMEM) with 10% fetal bovine serum (FBS) was added to quench the collagenase, and the solution was subsequently filtered in a 100 μm cell strainer (Falcon, 352360). The cells were pelleted by centrifugation (300 g, 7 min). The precipitated SVF cells were re-suspended in 1 mL Red blood cell lysis buffer (155 mM NH4Cl, 10 mM KHCO3,

0.1 mM EDTA, pH 7.3) for 2 min. A 10-fold excess of media was added prior to being filtered in a 40 μm cell strainer (Falcon, 352340). After centrifugation (300 g, 7 min) the cells were re-suspended in FACS staining buffer (PBS with 1% BSA and 2 mM EDTA).

Flow Cytometry of Murine Stromal Vascular Fraction

Stromal vascular fraction cells were stained in FACS staining buffer with the following fluorophore-conjugated primary antibodies F4/80 APC (BioRad, CI:A3-1), CD11b PE-Cy7 (BD Biosciences, MI/70), CD45 PE-CF594 (BD Biosciences, 30-F11), CD19 PE-Cy5 (Biolegend, 6D5), CD11c PE (BD Biosciences, HL3), Siglec-F BB515 (BD Biosciences, E50-2440). Cells were washed two times with staining buffer and suspended in FACS buffer (PBS with 0.5% BSA and 2 mM EDTA). The viability dye SYTOX Blue (ThermoFisher Scientific) and CountbrightTM Absolute Counting Beads (ThermoFisher Scientific) were added immediately before running the samples on a BD FACSAria Fusion. Data was analyzed in FlowJo (Tree Star).

Transcriptomic Array

Total RNA was quality checked on Agilent Technologies 2200 Tapestation. RNA quantity was measured using NanoDrop ND-1000 Spectrophotometer. Biotinylated DNA targets was prepared from 150 ng total RNA using the GeneChip WT Plus Reagent Kit according to the manufacturer's instructions. Hybridization, washing and staining was carried out on Clariom D Human arrays, using Affymetrix GeneChip Fluidics Station 450 according to the manufacturer's protocol. The fluorescent intensities were determined with Affymetrix GeneChip Scanner 3000 7G, and Affymetrix GeneChip Command Console (AGCC, v.4.1.2) was used to analyze the acquired array images. Gene-level SST-RMA processing and sample group comparisons were performed using Transcriptome Analysis Console (TAC, v.4.0). Nominally significant genes ($p < 0.01$) were analyzed in a gene ontology (GO) analysis performed using an online web tool (https://david.ncifcrf.gov/). The global WAT transcriptome of cohorts 1 and 2 have been previously described (Arner et al., 2012; Petrus et al., 2018b).

For the gene micro array identifying SP1 regulated genes, siRNAs targeting SP1 (pool of 3 siRNA; CTAGGACGCAATAAATTTATA, CAGCAAGTTCTGACAGGACTA, TCCCAGAAAGTATATACTGAA) or SiControl (both from QIAGEN, Germany) were transfected into human *in vitro* differentiated adipocytes at day 9 post-adipogenic induction using HiPerFect (QIAGEN, Germany). 96 h post-transfection, cells were lyzed and RNA was extracted with the MagMAX-96 for Microarrays Total RNA Isolation Kit (Thermo fisher scientific, Stockholm, Sweden). Gene expression profiling was performed using Affymetrix Human HTA 2.0 arrays (Affymetrix, Santa Clara, CA). Data were analyzed with packages available from Bioconductor (http://www.bioconductor.org/). Normalization and calculation of gene expression was performed with the Robust Multichip Average expression measure using oligo package. Prior to analysis, a non-specific filter was applied to include genes with expression signal > 30 in at least 20% of all samples. Limma package was used to identify differentially expressed genes between siSP1 and Sicontrol.

Chromatin Immunoprecipitation Sequencing

Chromatin immunoprecipitation (ChIP) was performed using the ChIP Assay Kit (Magna ChIP HiSens, Millipore) according to the manufacturer's instructions. Briefly, 1×10^7 adipocytes were fixed with 1% formaldehyde to cross-link histones to DNA. Cells were lysed with hypotonic buffer (0.2% NP40, 10 mM NaCl, 10 mM Tris-HCl (pH 7.5), 3 mM $MgCl_2$, 10 mM KCl_2). Isolated nuclei were resuspended in ChIP buffer (0.1% SDS, 1% Triton X-100, 0.15 M NaCl, 1 mM EDTA, 20 mM Tris-HCl) and subsequently sonicated in 30 cycles (30 s ON/OFF) in the Bioruptor Pico (Diagenode), to generate DNA-fragment sizes of 0.1 – 0.5 kb. The soluble chromatin supernatant was immunoprecipitated using anti-O-GlcNAc (RL2, Abcam ab2739), anti-SP1 (Abcam ab13370) or anti-mouse-IgG (Sigma-Aldrich). ChIP-sequencing (ChIP-seq) libraries were prepared using NEBnext chip-seq library Prep master mix set (New England Biolabs, Ipswich, MA). Sequence data were generated with Illumina HiSeq 2000 single-read sequencing and aligned against the human genome (hg38, NCBI) using Burrows-Wheeler Aligner (Li and Durbin, 2009) with default parameters. For O-GlcNAc, peak calling was performed with HOMER (v4.8, 1-13-2016, http://homer.ucsd.edu/homer/) to determine enrichment over the input samples across the whole genome. Peak size was optimized to 1000 bp, with the minimum distance to the next peak set to 2500 bp. The closest transcription start site (TSS) was then annotated to the enriched regions using HOMER, and differential analysis between treated and control samples were performed with edgeR (Bioconductor version 3.14.0, https://bioconductor.org/packages/release/bioc/html/edgeR.html). Pathway analysis of genes with differentially peak intensities in the proximity to their transcriptional start site were analyzed using an online web tool (https://david.ncifcrf.gov/). For SP1, sequence data were generated with Illumina Nextseq single-read sequencing and aligned against the human genome (hg38, NCBI) using STAR. Homer was subsequently used for peak calling, annotation and for counting tags within the identified peaks. The count table was imported into R/Bioconductor and statistical analysis was performed to identify differential peaks between the SP1 ChIP and background samples (IgG and input) using the EdgeR package and its general linear models' pipeline. Bedgraph files were produced using Homer and normalized to 10 million reads. ChIP-seqs were validated by ChIP-qPCR. ChIP enrichment was calculated as percentage of input. For ChIP-qPCR of SP1, two different anti-SP1 were used (Abcam ab13370, and Active Motif No:39058).

Cytokine Secretion

Conditioned media was collected at day 11 of human adipocyte differentiation and secreted levels of adipokines were assessed using Inflammation 20-plex Human panel (EXP200-12185-901, ProcartaPlex ThermoFisher Scientific) according to manufacturer's

instructions. Fifty microliters of each sample was analyzed by triplicates according to the standard protocol and data collected with MagPix (Luminex xMAP Corporation). Multiplex data for CCL2 and IL6 were confirmed by regular ELISA (ThermoFisher Scientific) as detailed in the Key Resources Table. For cells transfected with *siOGT*, conditioned media was obtained after 48 h of incubation (between day 9-11) while for cells treated with GalNAc-*O*-bn, PUGNAc and 2-DG, media was obtained after 24 h.

IL1B quantification was performed with V-plex Plus Human IL-1b kit (Mesoscale Discovery, K151QP, Research Boulevard, Rockville, US). Fifty microliters of each sample were analyzed according to manufacturer's instructions, data collected with SECTOR Imager 6000 and analyzed with MSD Discovery Workbench software.

Immunoprecipitation of O-GlcNAcylated Proteins

In vitro differentiated human adipocytes incubated with high and low glutamine were lysed at day 11 of differentiation with a hypotonic buffer (0.2% NP40, 10 mM NaCl, 10 mM Tris-HCl (pH 7.5), 3 mM MgCl2, 10 mM KCl_2) to enrich for nuclei. The nuclear extract was lysed by RIPA buffer isolate nuclear proteins which was then incubated with anti-O-GlcNAc (RL2, Abcam ab2739) or anti-mouse-IgG (Millipore) for 24 h, at 4°C. The antibody-proteins complexes were immobilized on magnetic Dynabeads protein G (ThermoFisher Scientific) for 4 h, at 4°C. Beads were washed with lysis buffer five times and eluted at 98°C for 10 min. Note that this isolation protocol is a standard operating procedure at the proteomics facility of the Karolinska Institute. It does not involve cross-linking and contains several wash steps to minimize the risk of unspecific protein binding. Nevertheless, as with any method, there is a balance between washing too little (with increased risk of detecting proteins through unspecific interactions) and too much (with the risk of not detecting O-GlcNAcylated proteins).

Western Blot Analysis

Samples were lysed in RIPA buffer supplemented with protease and phosphatase inhibitors and were diluted to a concentration of 20 μg of protein and heated at 95°C for 5 min with a denaturation buffer. Proteins were separated by SDS–PAGE electrophoresis and transferred to PVDF membranes (Amersham International, GE Healthcare). Membranes were incubated in blocking reagent (3% of Amersham ECL Prime Blocking solution reagent in tris-buffered saline-tween 20 (TBS-tween)) for 1 h, then in primary antibody (in the blocking solution) overnight at 4°C. The antibodies and their concentrations are the following: anti-O-GlcNAc (RL2, Abcam), anti-OGT (Active Motif), anti-GLUL (Sigma-Aldrich 2B12), anti-Lamin (Cell Signaling 4C11), anti-Actin (Sigma-Aldrich) and anti-α-Tubulin (Cell Signaling). After several washes in TBS-tween, membranes were incubated in horseradish peroxidase (HRP)-conjugated secondary antibodies for 1 h at room temperature in the blocking solution. Membranes were incubated with ECL western-blotting substrate (Amersham International, GE Healthcare) and imaged by in a Chemidoc XRS system or ChemiDOC (Bio-Rad Laboratories).

Glucose Uptake Assay and Seahorse Extracellular Flux Analysis

Glucose uptake was determined by measuring radioactivity within cells by liquid scintillation counting. The day before the assay, insulin was removed from culture medium. After two washes with PBS, cells were incubated 50 minutes at 37 °C. Then, 125 μM 2-deoxy-D-glucose and 0.4 μCi 2-DG per well were added for 10 minutes. Culture plates were put on ice and rinsed with 10 mM glucose in ice-cold PBS and then again with only ice-cold PBS. Cells were scraped in 0.05 M NaOH and 2-deoxy-D-glucose uptake was measured by liquid scintillation counting of cell lysate. Oxygen consumption rate (OCR) and extracellular acidification rate (ECAR) were measured by an XF96 Seahorse Extracellular Flux Analyzer (Agilent) following the manufacturer's instruction. For measurements of basal ECAR and OCR, cells were incubated in medium supplemented with 1 mM pyruvate, 2 mM glutamine and 10 mM glucose. To assess responses to glucose or glutamine addition, cells were incubated in medium without glucose or without glutamine respectively. During the assay, cells were treated with 10 mM glucose, 1 μM oligomycin, 50 mM 2-deoxyglucose, 2 mM glutamine, 3 μM BPTES. Each condition was performed with 4–6 replicates, and the readings of OCR and ECAR of each well were normalized to cell number.

Secreted Metabolomics Analysis

Biopsies from subcutaneous WAT (n = 29 in NO and n = 52 in OB) were incubated in Krebs Ringer Phosphate (KRP) supplemented with 2% bovine serum albumin, 1 mg/mL D-glucose and 0.1 mg/mL ascorbic acid (pH 7.4) for two h. Conditioned media were then kept at −80°C before analyses by untargeted metabolomics. In brief, on the day of analysis, the incubates (500 μl) were thawed in the refrigerator at 4°C (between 1:20 – 1:30 h). Samples were then vortexed for 30 s and 50 μL of sample were transferred to an Eppendorf tube. Next, 150 μL of LC-MS methanol (Optima, Fisherbrand) were added to each Eppendorf tube. Samples were then vortexed for 30 s and allowed to equilibrate for 10 min at room temperature. Afterward, samples were centrifuged at 12000 g for 15 min at 4°C). Then, 150 μL of the supernatant were filtered using Ultrafree-MC VV Centrifugal Filters (Merck-Millipore, LOT R6KA79803) at 5000 g for 3.5 min. Finally, two independent 50 μL aliquots were transferred to LC-MS vials. The remainder of the extracts was pooled for use as an MS injection quality control (QC). After pooling, the QC sample was aliquoted into 6 different LC-MS vials that were injected during the sequence (three for positive and three for negative mode).

LC-HRMS experiments were performed on a 1290 Infinity II ultra-high performance liquid chromatography (UHPLC) system coupled to a 6550 iFunnel quadrupole-time of flight (Q-TOF) mass spectrometer equipped with a dual AJS electrospray ionization source (Agilent Technologies, Santa Clara, CA). The polar secreted metabolites were separated on a SeQuant ZIC-HILIC (Merck,

Darmstadt, Germany) column 100 Å (100 mm × 2.1 mm, 3.5 μm particle size) coupled to a guard column (20 mm × 2.1 mm, 3.5 μm particle size) and an inline-filter. Mobile phases consisted of 0.1% formic acid in water (solvent A) and 0.1% formic acid in acetonitrile (solvent B). The elution gradient used was as follows: isocratic step at 95% B for 1.5 min, 95% B to 40% B in 12 min and maintained at 40% B for 2 min, then decreasing to 25% B at 14.2 min and maintained for 2.8 min, then returned to initial conditions over 1 min, and the column was equilibrated at initial conditions for 7 min. The flow rate was 0.3 ml.minutes^{-1}, injection volume was 2 μl and the column oven was maintained at 25°C.

Two independent injections were run for positive and negative acquisition modes. The Q-TOF MS system was calibrated and tuned according to the protocols recommended by the manufacturer. Nitrogen (purity > 99.999%) was used as a sheath gas and drying gas at a flow of 8 l minutes^{-1} and 15 l minutes^{-1}, respectively. The drying and sheath gas temperature were set at 250°C, with the nebulizer pressure at 35 psi and voltage 3000 V (+/− for positive and negative ionization mode, respectively). The fragmentor voltage was set at 380 V. The acquisition was obtained with a mass range of 50-1200 m/z, where full scan high-resolution data were acquired at three alternating collision energies (0 eV, 10 eV and 30 eV). The data acquisition rate was 6 scans.sec^{-1}. Between 0 and 1.5 min, LC flow was diverted to the waste. For further details regarding the acquisition methodology please see Naz et al. (2017).

Samples were processed using ProFinder B6.00.00 version using the in-house generated library with authentic standards (Naz et al., 2017). Compounds were identified according to their accurate mass and retention time matching to the library. For further confirmation, matching of compounds MS/MS spectra with those of the library was performed. After peak integration, samples were corrected using the quality control-robust spline correction algorithm implemented in MATLAB (Mathworks, R2015a) (Kirwan et al., 2013). The %CV for all reported metabolites was < 10.2% (average %CV = 3.4%). The %CV for glutamine was 3.2%. Conditioning media samples were extracted following the same protocol as the samples and injected at the beginning and the end of the sequence to check for any potential contribution to the detected metabolites (Daskalaki et al., 2018). Glutamine level contribution by the media was 6% of the total amount in the pooled samples.

Cellular Untargeted Metabolomics Analysis

Sample Preparation for Global Metabolomics

Sample preparation was carried out as described previously (Evans et al., 2009) at Metabolon. Briefly, recovery standards were added prior to the first step in the extraction process for quality control purposes. To remove protein, dissociate small molecules bound to protein or trapped in the precipitated protein matrix, and to recover chemically diverse metabolites, proteins were precipitated with methanol under vigorous shaking for 2 min (Glen Mills Genogrinder 2000) followed by centrifugation. The resulting extract was divided into five fractions: two (i.e., early and late eluting compounds) for analysis by ultra-high performance liquid chromatography-tandem mass spectrometry (UPLC-MS/MS; positive ionization), one for analysis by UPLC-MS/MS (negative ionization), one for the UPLC-MS/MS polar platform (negative ionization), and one sample was reserved for backup.

Three types of controls were analyzed in concert with the experimental samples: samples generated from a small portion of each experimental sample served as technical replicate throughout the dataset; extracted water samples served as process blanks; and a cocktail of standards spiked into every analyzed sample allowed instrument performance monitoring. Instrument variability was determined by calculating the median relative standard deviation (RSD) for the standards that were added to each sample prior to injection into the mass spectrometers (median RSD typically = 4%–6%; n ≥ 30 standards). Overall process variability was determined by calculating the median RSD for all endogenous metabolites (i.e., non-instrument standards) present in 100% of the pooled human plasma or client matrix samples (median RSD = 10%–14%; n = several hundred metabolites). Experimental samples and controls were randomized across the platform run.

Mass Spectrometry Analysis

Non-targeted MS analysis was performed at Metabolon. Extracts were subjected to UPLC-MS/MS (Evans et al., 2014). The chromatography was standardized and, once the method was validated no further changes were made. As part of Metabolon's general practice, all columns were purchased from a single manufacturer's lot at the outset of experiments. All solvents were similarly purchased in bulk from a single manufacturer's lot in sufficient quantity to complete all related experiments. For each sample, vacuum-dried samples were dissolved in injection solvent containing eight or more injection standards at fixed concentrations, depending on the platform. The internal standards were used both to assure injection and chromatographic consistency. Instruments were tuned and calibrated for mass resolution and mass accuracy daily.

The UPLC-MS/MS platform utilized a Waters Acquity UPLC with Waters UPLC BEH C18-2.1 × 100 mm, 1.7 μm columns and a Thermo Scientific Q-Exactive high resolution/accurate mass spectrometer interfaced with a heated electrospray ionization (HESI-II) source and Orbitrap mass analyzer operated at 35,000 mass resolution. The sample extract was dried then reconstituted in acidic or basic LC-compatible solvents, each of which contained 8 or more injection standards at fixed concentrations to ensure injection and chromatographic consistency. One aliquot was analyzed using acidic, positive ion-optimized conditions and the other using basic, negative ion-optimized conditions in two independent injections using separate dedicated columns (Waters UPLC BEH C18-2.1x100 mm, 1.7 μm). Extracts reconstituted in acidic conditions were gradient eluted using water and methanol containing 0.1% formic acid, while the basic extracts, which also used water/methanol, contained 6.5 mM ammonium bicarbonate. A third aliquot was analyzed via negative ionization following elution from a HILIC column (Waters UPLC BEH Amide 2.1x150 mm, 1.7 μm) using a gradient consisting of water and acetonitrile with 10 mM Ammonium Formate. The MS analysis alternated between MS and data-dependent MS2 scans using dynamic exclusion, and the scan range was from 80-1000 m/z.

Compound Identification, Quantification, and Data Curation

Metabolites were identified by automated comparison of the ion features in the experimental samples to a reference library of chemical standard entries that included retention time, molecular weight (m/z), preferred adducts, and in-source fragments as well as associated MS spectra and curated by visual inspection for quality control using software developed at Metabolon (Dehaven et al., 2010). Identification of known chemical entities was based on comparison to metabolomic library entries of purified standards. Peaks were quantified using area-under-the-curve. Raw area counts for each metabolite in each sample were normalized to correct for variation resulting from instrument inter-day tuning differences by the median value for each run-day, therefore, setting the medians to 1.0 for each run. This preserved variation between samples but allowed metabolites of widely different raw peak areas to be compared on a similar graphical scale. Missing values were imputed with the observed minimum after normalization.

Proteomics Profiling

The elution fraction after IP with anti-O-GlcNAc, anti-IgG (negative control) and input (positive control) antibodies were performed as described above. Samples were processed and analyzed at the proteomics core facility of Karolinska Institutet ("Proteomics Biomedicum at Karolinska Institutet"). In brief, this involved a number of steps listed below.

Protein Precipitation with Acetone and In-solution Digestion

Ice cold acetone in 4 x volume was added to 10 μg protein in Input samples (3 × 0.5 mM glutamine Input D11 and 3 × 10 mM glutamine Input D11) and incubated at −20°C overnight. Then the samples were centrifuged at 14000 g for 20 min and the supernatant was discarded. Acetone was allowed to evaporate in the open tubes at room temperature for 30 min. The pellets were dissolved in 10 μl of 8 M urea and sonicated for 10 min in ultrasonic bath and 70 μl of 100 mM ammonium bicarbonate (AmBic), pH 8 was added. Proteins were reduced with 5 mM dithiothreitol (DTT, Sigma-Aldrich) and incubated at 37°C for 45 min. Alkylation was performed with 15 mM iodoacetamide (IAM, Sigma-Aldrich) at room temperature for 30 min in dark. Then 0.4 μg of sequencing grade modified trypsin (Promega) was added to each sample (1:25 trypsin:protein) and incubated at 37°C for 16 h. The digestion was stopped by adding formic acid at final concentration of 5%. Then the samples were cleaned on a C18 Hypersep plate (Thermo Scientific) and dried using a speedvac (MiVac; Thermo Scientific).

Washing Beads and On-beads Digestion

Aliquots of 50 μl Dynabeads (Protein G) with mouse IgG1 were used for the IP samples. The buffer was discarded after magnetizing the beads and washed them two times with 250 μl of 50 mM AmBic, pH 8. Beads were incubated at RT in shaker (350 rpm) for 15 min and then centrifuged and magnetized before discarded the buffer after each wash. Finally, the beads were resuspended in 70 μl of 50 mM AmBic, pH 8. Proteins were reduced with 10 mM DTT (Sigma-Aldrich) and incubated at 37°C for 45 min. Alkylation was performed with 30 mM IAM (Sigma-Aldrich) at room temperature for 30 min in dark. Then 2 μg of sequencing grade modified trypsin (Promega) was added to each sample and incubated at 37°C for 16 h. Beads were magnetized for 30 s and supernatants were transferred to new tubes. Further digestion was performed on the beads with 0.4 μg of trypsin at 37°C for 2 h. Beads were again magnetized for 30 s and supernatants were transferred to first tube. The digestion was stopped by adding formic acid at final concentration of 5%. Then the samples were cleaned on a C18 Hypersep plate (Thermo Scientific) and dried using a speedvac (MiVac; Thermo Scientific).

TMT6plex-Labeling

Samples were dissolved in 50 mM triethylammonium-bicarbonate (TEAB), pH 8 while TMT6plex reagents were dissolved the in dry acetonitrile. Samples were scrambled, then incubated at RT, 550 rpm for 2 h. The reaction was stopped by adding hydroxylamine at final concentration of 0.5% incubated for at RT with 550 rpm for 15 min. Individual samples were combined to one analytical sample and dried in speedvac, followed by cleaned up on C18 Stage Tips and dried again in speedvac.

PRLC-MS/MS Analysis

Chromatographic separations of peptides were performed on an EASY-spray column connected to an EASY-nLC1000 system (Thermo Fisher Scientific). Eluted with a 90 min gradient at a flow rate of 300 nL/minutes and a Fusion Orbitrap mass spectrometer (Thermo Scientific) analyzed the eluted peptides that were ionized with electrospray ionization. The survey MS spectrum was acquired at the resolution of 60,000 in the range of m/z 350-1800. MS/MS data were obtained with a higher-energy collisional dissociation (HCD) for ions with charge $z > 1$ at a resolution of 30,000 and first mass at m/z 100. The gradient went from 2%–26% of buffer B (2% acetonitrile, 0.1% formic acid) in 80 min, up to 35% of buffer B in 10 min and up to 95% of buffer B in 2 min and the effluent was electrosprayed into the mass spectrometer direct via the column.

Data Analysis

The raw files were converted to Mascot Generic Format (mgf) using the in-house written Raw2mgf program. Proteins were identified by searching mgf files against the SwissProt database (HUMAN) using Mascot v 2.5.1 (MatrixScience Ltd., UK) database search engine. Pathway and cluster analyses were performed using a web tool (https://string-db.org/cgi/network.pl).

QUANTIFICATION AND STATISTICAL ANALYSES

Values are mean ± Standard Error of the Mean (SEM) if not otherwise stated. All datasets were tested for normal distribution using Shapiro-Wilk tests. Skewed data were log-transformed. Results were evaluated using unpaired (2-sided) t test, Welch's two-sample t test and one- or two-way analysis of variance (ANOVA). Tukey's post hoc test was used. For analyses of glutamine handling genes in array data from cohort 2, Bonferroni correction was used. Array and ChIP-seq data were analyzed as described under the respective

paragraphs. For correlation analyses Pearson's correlation coefficient were used or multiple regression analyses when BMI corrections were made. Statistically significant differences were considered to be $p < 0.1$ (Welch's test), $p < 0.05$ or $p < 0.01$ depending on the analysis performed. The relevant statistical methods for each panel are detailed in the figure legends. All statistical analyses (except omics data) were performed using GraphPad or SPSS.

DATA AND CODE AVAILABILITY

Gene microarray and ChIPseq data have been uploaded to the Gene Expression Omnibus (GEO) under the following accession numbers: i) GEO: GSE59034; microarray of adipose tissue from the clinical cohort, ii) GEO: GSE140426; microarray of human *in vitro* differentiated adipocytes incubated in high and low glutamine, SP1 RNAi in human *in vitro* differentiated adipocytes and O-GlcNAc ChIPseq.